Biochimica et Biophysica Acta, 1016 (1990) 293–327
Elsevier

BBABIO 43187

Review

Nature of the primary photochemical events in rhodopsin and bacteriorhodopsin

Robert R. Birge

Department of Chemistry, Syracuse University, Syracuse, NY (U.S.A.)

(Received 4 August 1989)

Key words: Rhodopsin; Bacteriorhodopsin; Primary event; Photochemistry

Contents

Abbreviations: B, bathorhodopsin; bR, light-adapted bacteriorhodopsin; {J, K, L, M, N, O}, intermediates in the photocycle of light adapted bacteriorhodopsin; I, isorhodopsin; Lumi, lumirhodopsin; {Meta I, II, III}, metarhodopsin I, II or III; R, vertebrate rhodopsin; UV-Vis, ultraviolet and visible; f, one-photon oscillator strength; δ, two-photon absorptivity; GM, Goeppert-Mayer two-photon absorptivity unit ($1 \cdot 10^{-50}$ cm$^4 \cdot$s$\cdot$mol$^{-1} \cdot$photon^{-1}); Amino acid abbreviations are as follows: Ala, A, alanine; Arg, R, arginine, Asn, N, asparagine; Asp, D, aspartic acid; Cys, C, cysteine; Gln, Q, glutamine; Gly, G, glycine; His, H, histidine; Ile, I, isoleucine; Leu, L, leucine; Lys, K, lysine; Met, M, methionine; Phe, F, phenylalanine; Pro, P, proline; Ser, S, serine; Thr, T, threonine; Trp, W, tryptophan; Tyr, Y, Tyrosine; Val, V, valine.

Correspondence: R.R. Birge, Department of Chemistry, Syracuse University, Syracuse, NY 13244, U.S.A.

I. Introduction

Rhodopsin, the protein responsible for converting light into an optic nerve impulse, and bacteriorhodopsin, the light transducing protein of the purple membrane of *Halobacterium halobium,* have significantly different biological roles. Nevertheless, natural selection has converged on very similar designs for both proteins, and these similarities have prompted comparative experimental and theoretical studies. The nature of the primary photochemical events in rhodopsin and bacteriorhodopsin has been the subject of extensive research during the past decade. The lack of high-resolution X-ray structural data has precluded an assignment of the tertiary structure of either protein, and hence our knowledge of the binding sites and the primary events is based on indirect analyses of chemical and spectroscopic data. Despite a number of important advances during the past decade, however, much remains to be explained and a number of interesting experimental paradoxes remain unexplained. The goal of this review is to explore these controversies and paradoxes in sufficient detail to provide researchers with the background critical to an appreciation of the experimental and theoretical issues. Thus, this review is selective and not comprehensive. The interested reader may consult Refs. 11, 29, 39, 73, 101, 138, 140, 151, 186, 187, 188, 219, 276, 289, 308, 312 for more detailed reviews of those issues not covered fully in this discussion.

II. Structure and function of rhodopsin and bacteriorhodopsin

This section overviews the known primary and presumed secondary and tertiary structures of vertebrate rhodopsin and light adapted bacteriorhodopsin. We also examine the in vivo functioning of both proteins in order to provide a framework for a more detailed analysis of the primary photochemical events.

Rhodopsin ($M_r \approx 40\,000$) is the protein responsible for generating an optic nerve impulse in the visual receptors of the three phyla that possess image-resolving eyes: mollusks, arthropods and vertebrates. Despite what is believed to be independent evolutionary development, these three phyla have converged on a remarkably similar protein structure and an identical light-absorbing chromophore, 11-*cis*-retinal. The generation of a nerve impulse following excitation of rhodopsin involves a complex series of reactions which ultimately hyperpolarize the plasma membrane of the rod cell in the retina [193,312]. The plasma membrane contains numerous cation-specific channels which are open to sodium ion flow in the dark. Light sets off a series of biochemical reactions which block these channels, and the resultant hyperpolarization generates a more negative potential inside the cell. The key feature of this event is that a single photon of light can generate a hyperpolarization of close to 1 mV (about 10^6 Na^+ ions blocked), which is sufficient to activate a nerve impulse in a dark adapted retina. (In practice, about 100 photons must enter the eye in order to generate an observed reproducible physiological response (see subsection IV-F). Light adaptation decreases this sensitivity level further.) The significant amplification factor in the hyperpolarization of the plasma membrane is accomplished via a complex biochemical reaction cycle involving transducin, a peripheral membrane protein of the G-protein family. A single molecule of photoactivated rhodopsin (R*) catalyzes the activation of up to 1000 transducin molecules ($T_{\alpha\beta\gamma}$-GDP + R* → R*-$T_{\alpha\beta\gamma}$-GDP + GTP → R*-$T_{\alpha\beta\gamma}$-GTP + GDP), and represents the initial stage in the amplification process. The second stage of amplification involves a splitting off of the α subunit of transducin from the β and γ subunits, and activation of phosphodiesterase (PDE) by the α subunit (PDE + R*$T_{\alpha\beta\gamma}$-GTP → PDE + T_α-GTP + R* + $T_{\beta\gamma}$ → PDE* + R* + $T_{\beta\gamma}$). (The binding of GTP to transducin releases activated rhodopsin (R*) for continued catalytic activity via the initial stage.) The activated phosphodiesterase complex (PDE*-T_α-GTP) hydrolyzes cyclic GMP (c-GMP) to 5′-GMP which closes the sodium ion channels {c-GMP + H_2O + open channel(s) → 5′-GMP + H^+ + closed channel(s)}. The transducin cycle returns to the starting point through deactivation of phosphodiesterase via hydrolysis of GTP bound to T_α and recombination of the β and γ subunits with T_α (PDE*-T_α-GTP + $T_{\beta\gamma}$ → PDE + $T_{\alpha\beta\gamma}$-GDP). Two mechanisms operate to close down the cascade and regenerate the resting state in preparation for reactivation by a subsequent photon absorption event. Activated rhodopsin (R*) is removed through phosphorylation followed by the binding of arrestin (An) (R* + ATP + An → R*-P + ADP + An → An-R*-P). Arrestin is an inhibitory protein that blocks the binding of transducin to photoactivated rhodopsin. The second mechanism involves restoration of the open channels via catalysis of GTP with guanylate cyclase (GC) followed by hydrolysis of pyrophosphate (PP) (closed channels + GTP + GC + H_2O → c-GMP + PP + H_2O → c-GMP + 2P + open channels).

Bacteriorhodopsin ($M_r \approx 26\,000$) is the light transducing protein in the purple membrane of *Halobacterium halobium* [241,242,243,310]. This halophilic archaibacterium grows in salt marshes where the concentration of the NaCl can exceed 4 M, roughly 6-times higher than seawater (about 0.6 M NaCl). The purple membrane, which contains the protein bacteriorhodopsin in a lipid matrix (3 : 1 protein : lipid), is grown by the bacterium when the concentration of oxygen in the salty water becomes too low to sustain the generation of ATP via oxidative phosphorylation. This is a common occur-

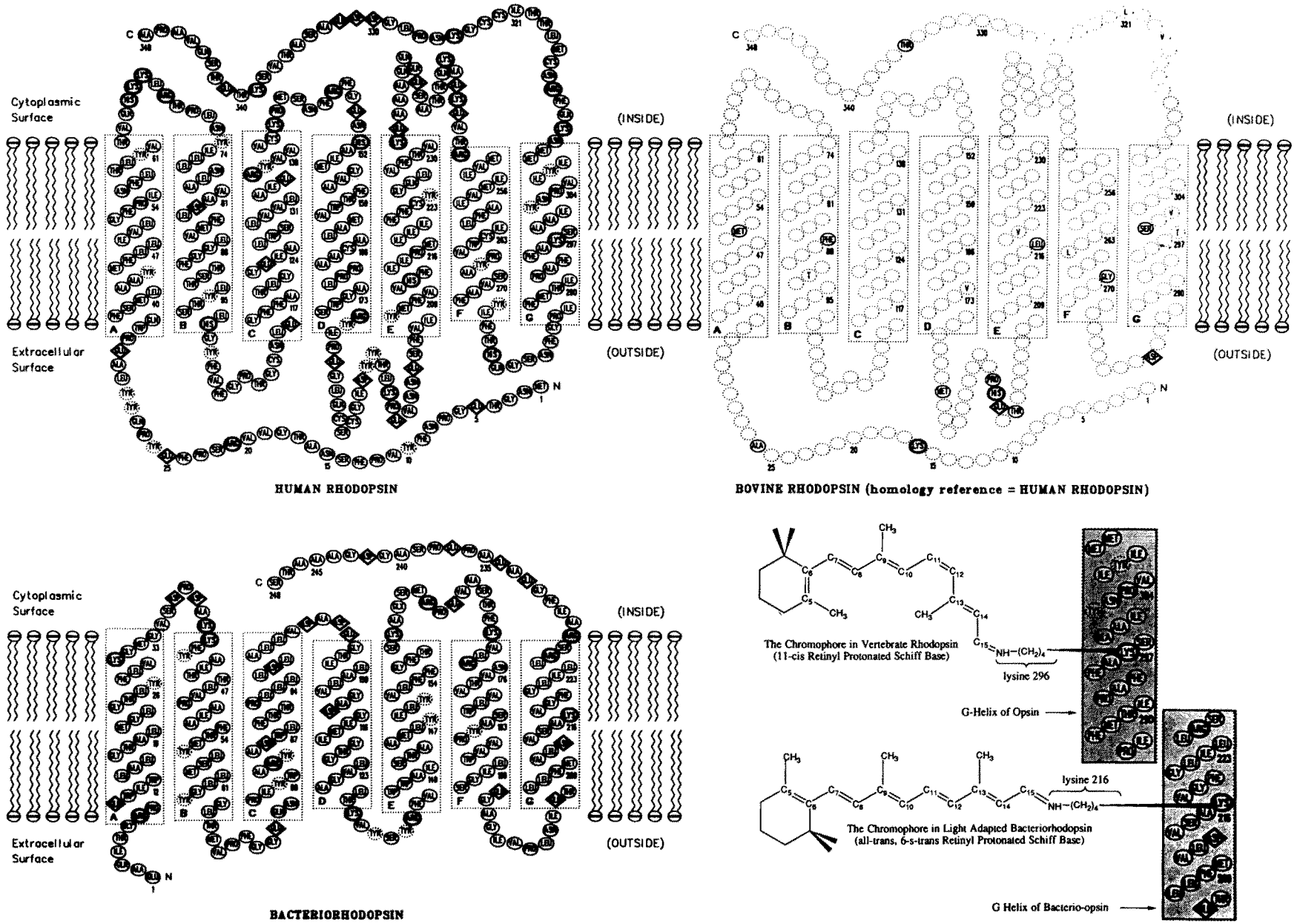

Fig. 1. Amino acid sequences and putative membrane spanning regions of human rhodopsin (upper left) and bacteriorhodopsin (lower left). The conformations and lysine residue attachment loations of the retinyl chromophores are shown at lower right. The diagram at upper right examines the homology between bovine rhodopsin and human rhodopsin. Only those amino acids in the bovine protein which differ from those found in the human protein are indicated. One letter codes are used to indicate amino acids with similar properties and three letter abbreviations are used to indicate amino acids which have significantly different characteristics relative to the corresponding human protein.

rence in hot salt water, and thus marshes containing large populations of this bacterium are typically a deep red in color. The lipid is a complex mixture of about 40 constituents. It includes a full set of enzymes for synthesizing carotenoids and retinal and the lipid portion is composed of 50% diether analog of phosphatidylglycerophosphate, 30% sulfoglycolipid, 6% carotenoids and assorted apolar lipids. Upon the absorption of light, bacteriorhodopsin converts from a dark adapted state to a light-adapted state. Subsequent absorption of light by the latter generates a photocycle which pumps protons across the membrane, with a net transport from the inside (cytoplasmic) to the outside (extracellular) of the membrane. The resulting pH gradient ($\Delta pH \approx 0.2$) generates a protonmotive force which is used by the bacterium to synthesize ATP from inorganic phosphate and ADP. Halobacterium halobium is thus capable of either respiratory or photochemical ATP synthesis, a flexibility that is rather unique among both simple and complex organisms.

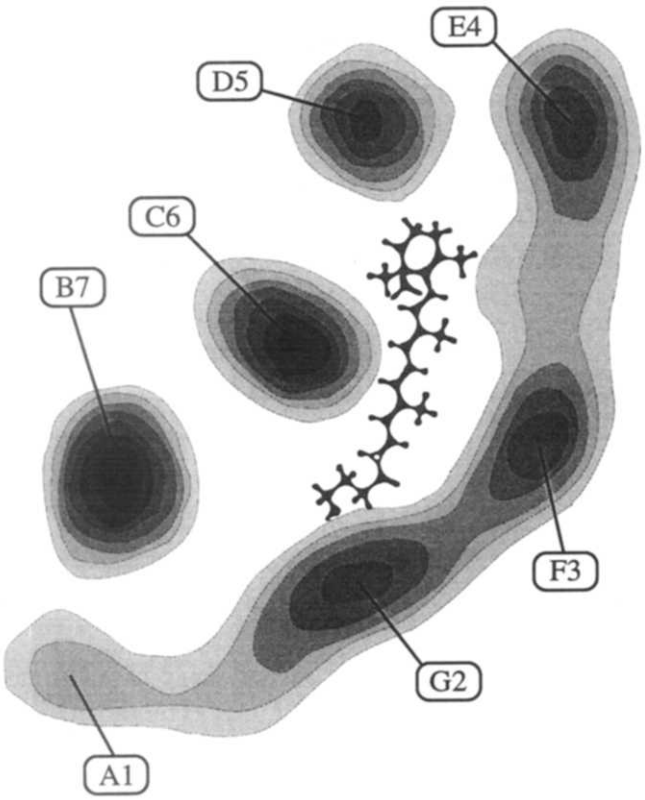

Fig. 2. Electron density profiles (data from Ref. 141) of bacteriorhodopsin viewed from the cytoplasmic side showing the seven transmembrane spanning segments and the presumed location of the chromophore in relation to the helices based on the available experimental data (see text). FTIR studies indicate that the polyene chain of the retinyl chromophore in bacteriorhodopsin lies roughly perpendicular to the membrane plane [99]. The retinyl chromophore is rotated artificially into the membrane plane to more clearly show the polyene chain (the imine nitrogen is indicated with an open circle) and the β-ionylidene ring. The conformation of the lysine residue is tentative [53].

II-A. Organization of the proteins in the membrane

The primary sequences of rhodopsin and bacteriorhodopsin, and the assumed organization of the proteins in their respective membranes, are shown in Fig. 1. Spectroscopic and low resolution diffraction studies on bacteriorhodopsin have indicated that the protein spans the membrane seven times [2,28,35,39,108,109,141–146, 178,187,247,248,310,311]. These studies have not shown conclusively the relationship between membrane spanning segments (A...F in Fig. 1) and the electron density profiles shown in Fig. 2, but the studies of Heyn et al. [145,146] and Agard and Stroud [2] suggest the assignments presented in Fig. 2. The all-*trans* retinal Schiff base chromophore is covalently bound to baterio-opsin via a protonated Schiff base linkage to lysine 216 on helix G (Fig. 1) [35,178,247,248]. The chromophore spans the intrahelical region shown in Fig. 2, and thus has potential nearest-neighbor interactions with five of the seven helices C, D, E, F and G. Because the primary event involves an all-*trans* to 13-*cis* photoisomerization, the model shown in Fig. 2 suggests that the key chromophore–protein interactions are with helices C, F and G. The primary counterion interacts with the C_{13}=C_{14}–C_{15}=NH– portion of the chromophore in bacteriorhodopsin, and as noted below, it is likely to be either Tyr-185 or Asp-212, although Asp-85 is also a possibility. Indeed, all three may provide some degree of stabilization of the protonated Schiff base chromophore in the binding site as proposed by Braiman et al. [68]. Furthermore, it is possible that the primary counterion changes during the photocycle, and that two forms of light-adapted bacteriorhodopsin may exist, with the key difference involving a switch in the primary counterion (see below).

We know much less about the structure of rhodopsin in the membrane, but spectroscopic and neutron diffraction studies, amino acid composition and analogies with bacteriorhodopsin suggest the secondary structure shown in Fig. 1 [1,138,139,140]. Thus, rhodopsin spans the membrane seven times and it is likely that the 11-*cis* chromophore linked to Lys-296 spans an intrahelix region similar to that shown in Fig. 2 for bateriorhodopsin. There are four amino acids which are candidates for the single primary counterion: Asp-83 (B helix), Glu-113 (C helix), Glu-122 (C helix) and Glu-134 (C helix). We know from one-photon [51] and two-photon [57] spectroscopic studies that the key perturbations involve C_{13}-CTN and C_{15}-CTN chromophore-counterion (CTN) interactions. Recent site directed mutagenesis studies indicate that Glu-113 is the primary counterion [274] (see subsection III-B).

II-B. The photobleaching sequence of rhodopsin

At ambient temperature and neutral pH, rhodopsin undergoes the photobleaching sequence shown in Fig. 3. The rhodopsin to bathorhodopsin phototransformation represents the so-called 'primary event' or 'primary photochemical event'. (It is perhaps misleading to use the latter term, because there are no *secondary* photochemical events. Nevertheless, it has become a commonly used expression, and should be interpreted to mean a primary event involving a photochemical transformation.) The primary event stores about 32 kcal · mol^{-1} of energy [74,75,277], and all subsequent reactions are thermal. It is now firmly established that the primary event involves an 11-*cis* to 11-*trans* photoisomerization [54,55,129,152,263]. There is a precursor to bathorhodopsin, known as hypsorhodopsin, but the biological relevance of this 'intermediate' remains a subject of debate, because it is formed preferentially under high light intensities [179,222,250]. Thus it may be an experimental artifact due to multiphoton processes. More recently, a ground-state precursor to bathorhodopsin, called photorhodopsin (or P-Batho) has been identified [290,329]. This precursor is discussed in more detail in Section IV. A key difference between rhodopsin and bacteriorhodopsin is that the final reaction in the photobleaching process of rhodopsin involves expulsion of the isomerized chromophore from the protein binding site. This denaturation precludes a rapid recycling of the protein, because an enzyme (retinyl ester isomerase) is required to reisomerize the all-*trans* chromophore to 11-*cis*-retinal prior to regeneration of the protein [189]. The total process takes about 20 min, and this time differential is utilized in vivo for light adaptation. Resonance Raman [72,73,82,110,219,246,249], FTIR [81,233,267,294] and other experimental studies [51,57,121,127,205,328] indicate that the chromophore is protonated in rhodopsin, bathorhodopsin, lumirhodopsin, metarhodopsin I and metarhodopsin III and is deprotonated in metarhodopsin II. It is now generally believed that the meta I → meta II transition initiates the transducin cycle responsible for the optic nerve impulse (see previous section). Longstaff et al. [203,205] have demonstrated that all of the lysine residues of rhodopsin, with the exception of Lys-296 to which the chromophore is attached, can be dimethylated without destroying biochemical activity. In contrast, monomethylation of Lys-296 blocks the meta I → meta II transition by preventing deprotonation of the retinyl Schiff base, and more interestingly, prevents activation of the G protein. Thus, deprotonation of the chromophore is required for generation of the optic nerve impulse. It is difficult to reconcile this observation with recent studies on phototaxis in *Chlamydomonas reinhardtii,* a unicellular alga which contains a rhodopsin-like protein [114–116]. Foster and co-workers have studied close to 100 chromophore analogs incorporated into *Chlamydomonas* opsin, and have shown that a majority show phototaxis, even when no 'isomerizable' chromophore is incorporated [114,115]. Thus, a photocycle involving photoisomerization appears to be unnecessary for *Chlamydomonas* rhodopsin activation. We will discuss the relevance of this observation to visual rhodopsin activation in further detail below.

II-C. The photocycle of bacteriorhodopsin

At ambient temperatures under low-light conditions, the purple membrane of *Halobacterium halobium* contains a binary mixture of two proteins, one containing 13-*cis*-retinal and the other containing all-*trans* retinal. The protein containing 13-*cis*-retinal is known as dark-adapted bacteriorhodopsin and the protein containing all-trans retinal is known as light-adapted bacteriorhodopsin. (It should be noted that many authors refer to the equilibrated mixture of all-*trans* and 13-*cis* proteins that spontaneously forms in the absence of light as 'dark-adapted bacteriorhodopsin'. Thus, one must be careful to determine from the individual paper which convention is being used.) The latter protein undergoes the photocycle shown in Fig. 3, and is the only form of the protein which pumps protons. Thus, light-adapted bacteriorhodopsin is the biologically active form and in all future discussions in this review, we will often refer to light-adapted bacteriorhodopsin simply as bacteriorhodopsin, or bR.

The phototransformation of bR to K is the 'primary event'. The primary photoproduct, K, stores about 16 kcal · mol^{-1} [49,50,52] and involves an all-*trans* to 13-*cis* photoisomerization of the protonated Schiff base chromophore [7,111,156,184,220,319]. There is at least one known precursor to K, called J, but we assign K as the primary photoproduct because J is not stable, even at liquid helium temperatures. It has also been proposed that J may represent a mixture of ground and trapped excited state species [53], but this hypothesis remains controversial. Recent experiments indicate that there are at least six intermediates following K [327], and thus the photocycle shown in Fig. 3 is an oversimplification. The search for new intermediates remains an area of active study.

The key thermal intermediate in the photocycle is M, because the formation of this intermediate coincides with the pumping of the proton [65,192,204,209,244, 269,310,311]. Resonance Raman [9,10,67,83,147,160, 219,221,300,309,317], FTIR [3,81,99,105,122,233,260–262,265,267,269,294] and other experimental investigations have established that the chromophore is protonated in all intermediates except M.

Two key issues regarding the photocycle that remain unresolved are the quantum yield of the primary event and the number of protons pumped per photocycle. We will examine these two issues in detail in Section V.

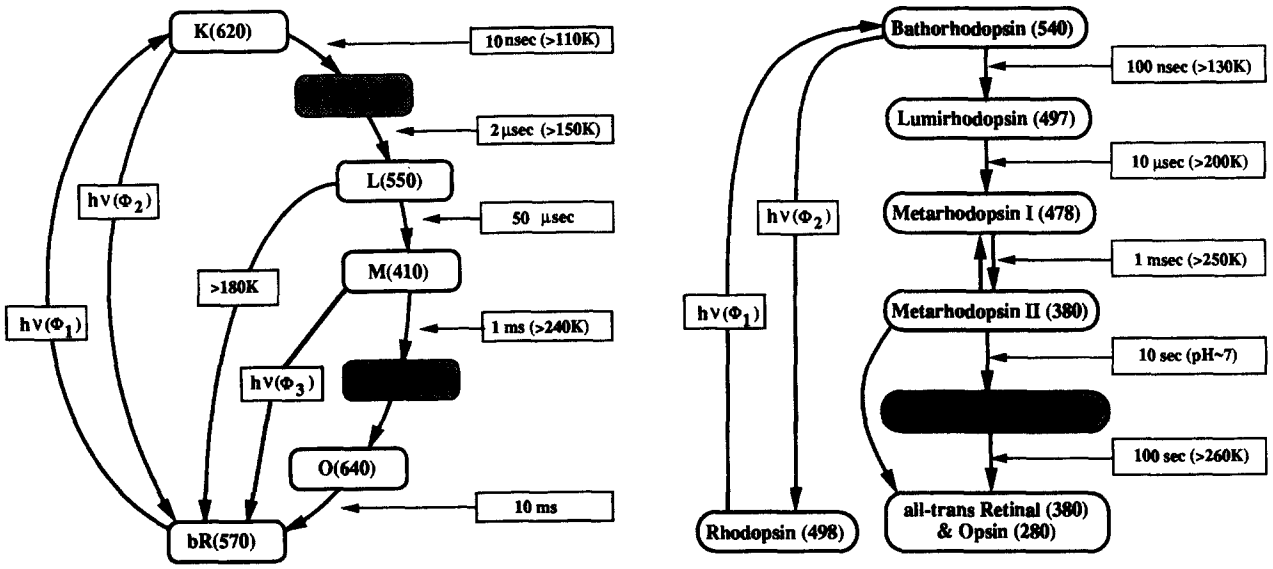

Fig. 3. Photocycle of light-adapted bacteriorhodopsin (left) and photobleaching sequence of vertebrate rhodopsin (right). Individual species are indicated within the polygons and the numbers in parentheses following the labels indicate the approximate absorption maximum in nanometers extrapolated to ambient temperature. Species within shaded polygons are tentative and/or are not observed under all experimental conditions. Species that cannot be trapped at low temperatures are not shown. Accordingly, J (an unstable species that precedes K) and photorhodopsin (an unstable species that precedes bathorhodopsin) are not included. Relative free energies are related approximately to vertical position. Temperatures required for observing the formation of subsequent intermediates and formation times extrapolated to ambient temperature are indicated for selected reactions, and are very approximate. A few key thermal and photochemical branching reactions are shown.

III. Nature of the protein binding sites of rhodopsin and bacteriorhodopsin

A detailed examination of the primary photochemical event must start with a realistic model of the binding site, and in particular, the specific chromophore–protein interactions that are responsible for stabilizing the ground state protonated Schiff base retinyl polyene. The lack of high resolution diffraction data on rhodopsin and bacteriorhodopsin, however, has precluded definitive assignment of the binding site geometries in either protein. Nevertheless, spectroscopic, site directed mutagenesis and chromophore analog studies have provided insights into the nature of the binding sites. We overview these experimental studies in the following two sections prior to presenting models of the binding sites.

Theoretical studies have also made important contributions to our perspective on the binding sites and the primary photochemical events. For convenience, we will discuss the theoretical literature at various points throughout this review rather than isolating it in a separate section. As demonstrated below, theory has contributed significantly to the analysis and interpretation of spectroscopic data on both the isolated chromophores [45,62,88,154,157–159,174,272,301,322] and the protein bound chromophores [44,47,50–55,57,80,87, 151–156,159,174,175,231,234,255,264,296,302,306,323–325,331].

III-A. Spectroscopic investigations of the binding site

Spectroscopy has played a key role in the experimental investigation of the binding sites of rhodopsin and bacteriorhodopsin. The following discussion is limited primarily to a selection of key spectroscopic observations of the past 5 years. For convenience, we have organized our discussion by technique rather than by protein.

Electron microscopy and neutron diffraction

The pioneering studies of Henderson and coworkers provided the first three-dimensional models of the purple membrane by using electron microscopy [109,142, 143,144]. Additional electron microscopy studies by Hayward et al. [141] and Agard and Stroud [2] as well as a number of neutron diffraction investigations [145, 146,273,282] are consistent with the helix assignments shown in Fig. 2. The recent neutron diffraction studies of Heyn et al. [145,146] are particularly noteworthy and provide a well-defined assignment of the chromophore location within the membrane spanning helices (Fig. 2). High resolution studies by Baldwin et al. indicate that all seven membrane spanning segments have α-helical secondary structure [28].

Circular dichroism spectroscopy

The recent book by Shichi provides an excellent discussion of the application of circular dichroism to an

analysis of rhodopsin [289]. Most studies on bacteriorhodopsin have supported the concept that the membrane spanning regions are α-helical and have little, if any, β-sheet content (for an excellent discussion see Ref. 232). However, many investigators interpret the CD spectra to indicate that one or two membrane spanning segments contain significant β-sheet content [94,173,190]. As noted above, however, the presence of β-sheet segments is not supported by diffraction studies.

UV-Vis electronic spectroscopy

Electronic (one-photon) absorption spectra of rhodopsin and bacteriorhodopsin are shown in Fig. 4,

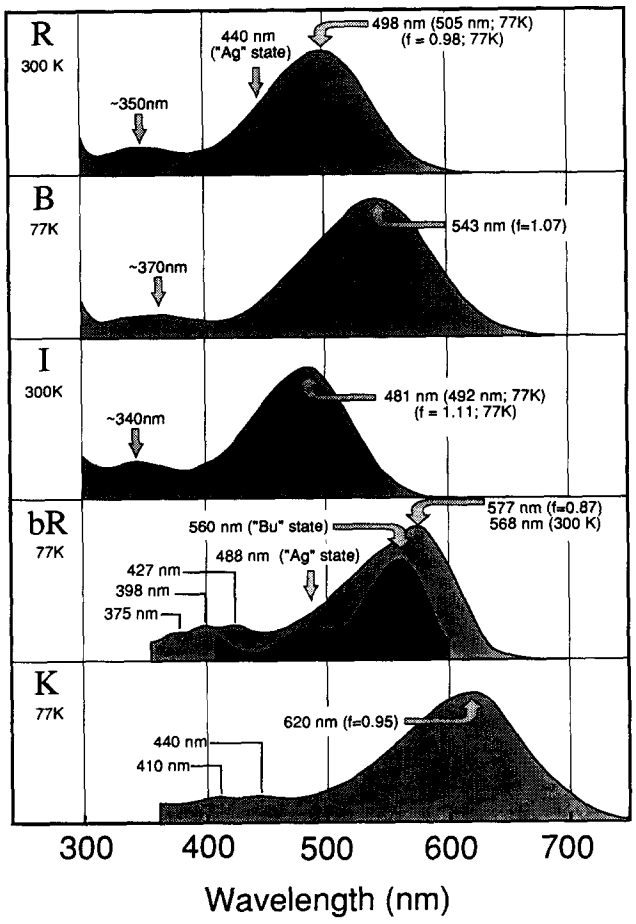

Fig. 4. Electronic (one-photon) absorption spectra of rhodopsin (R), bathorhodopsin (B), isorhodopsin (I), light adapted bacteriorhodopsin (bR) and K. Temperatures of the one-photon spectra are shown below the labels. The two-photon thermal lens spectrum of rhodopsin and the two-photon double resonance spectrum of bacteriorhodopsin (both in D_2O at room temperature) are shown in darker insets. The two-photon spectra have been shifted to lower absorptivity so that only the maxima are shown. The 'Ag' labels indicate two-photon maxima assigned to $'^1A_g^{*-}' \leftarrow S_0$ transitions and the 'Bu' labels indicate two-photon maxima assigned to $'^1B_u^{*+}' \leftarrow S_0$ transitions (see text). Oscillator strengths (f) determined by log-normal fits of the λ_{max} bands are indicated in parentheses. One photon spectra are from Refs. [50,51,77] and two-photon spectra are from Refs. 57, 331.

and the key spectroscopic results are presented in Table I. Note that some of the spectra shown in Fig. 4 are taken at liquid nitrogen (77 K) temperature. In the case of the primary photoproducts (bathorhodopsin and K), the most reliable spectra are those taken at temperatures for which the photoproducts are stable. We have shown a liquid nitrogen spectrum of bR because it exhibits more clearly resolved vibronic structure in the higher energy band.

All of the pigment spectra display two absorption bands, a strong, unresolved λ_{max} band in the green-red region and a weaker band in the blue region. A third intense band at about 280 nm (not shown) is also present in all pigment spectra, but is due to aromatic amino acids and not chromophore transitions. There are three low-lying π,π^* electronic states which are of particular importance to an analysis of the one-photon and two-photon spectra of both the isolated and protein-bound visual chromophores: $'^1B_u^{*+}'$, $'^1A_g^{*-}'$, $'^1A_g^{*+}'$. The quotation marks are to indicate that the symmetry labels are approximate. The labels are derived by reference to the corresponding states in a linear polyene (C_{2h} symmetry) [38,40,43–46,51,57,58,62,88,154,163,164,231]. The $'^1B_u^{*+}'$ state is a strongly allowed state in all polyenes, and in the case of linear polyenes, it is the only low-lying allowed state. The $'^1A_g^{*-}'$ state is a forbidden state which gains intensity in lower symmetry polyenes through coupling with the $'^1B_u^{*+}'$ state. Assignment of this state in inhomogeneously broadened systems is normally only possible by using two-photon spectroscopy [40,42–44,57,59,61,231], although crystal studies have also been successful [96,97]. The $'^1A_g^{*+}'$ state is responsible for the so-called '*cis*-band' in polyenes [154]. In non-polar polyenes it gains intensity via *cis* linkages, and the closer the *cis* linkage to the center of the polyene chain, the more intense the $'^1A_g^{*+}' \leftarrow S_0$ transition. In polar polyenes, it gains intensity not only from *cis* linkages but also from dipole–dipole interactions, and the larger the dipole moment, the more intense the $'^1A_g^{*+}' \leftarrow S_0$ transition. A more detailed discussion of the nature of these states may be found in the following references [38,40,43–46,51,57,58,62,88,96,97,154,163,164,231].

A great deal can be learned by analyzing the allowedness of an electronic transition. The allowedness is defined in terms of a dimensionless parameter known as the oscillator strength, which is represented by the symbol f. By using log-normal curve fitting procedures [224] it is possible to assign the oscillator strength with reasonable accuracy (Fig. 4, Table I, and Ref. 51). If one knows both the absorption maximum and the oscillator strength of an electronic transition, theoretical analysis of this data pair provides a perspective on the geometry of the chromophore and the nature of the protein-chromophore interactions. Birge and coworkers have examined the oscillator strength data for both

TABLE I

Spectroscopic properties of selected isomers of the visual chromophore, and the primary photoproducts of vertebrate rhodopsin and light-adapted bacteriorhodopsin at 77 K and 296 K

Data are taken from Refs. 22, 34, 39, 44, 49, 50, 51, 58, 136, 154, 211, 258, 277, 306, 320. Note that for the visual chromophores, all data at 77 K are for the aldehydes in EPA (ethyl ether/isopentane/ethyl alcohol; 5 : 5 : 2, v/v) and all data at ambient temperature (296 K) are for the protonated Schiff bases in methanol. The pigment spectra were collected in glycerol/H_2O (77 K) or H_2O (296 K).

Property	Visual chromophores				Bovine rhodopsin			*H. halobium*	
	all-*trans*	9-*cis*	11-*cis*	13-*cis*	Rho	Batho	Iso	bR	K
Isomer	all-*trans*	9-*cis*	11-*cis*	13-*cis*	11-*cis*	all-*trans*	9-*cis*	all-*trans*	13-*cis*
6-s-geometry	*cis*	*cis*	*cis*	*cis*	*cis*	*cis*	*cis*	*trans*	*trans*
77 K (EPA/glycerol):									
λ_{max} (nm)	387	380	389	382	505	543	492	577	620
ΔE_{max} (eV) ($\times 10^2$)	320	326	319	325	246	228	252	215	200
ϵ_{max} ($M^{-1} \cdot cm^{-1}$) ($\times 10^{-2}$)	526	432	457	442	464	525	486	661	639
f (λ_{max} band) ($\times 10^2$) [a]	117	98	104	106	98	107	111	87	95
$\Delta\nu_{FWHM}$ (cm^{-1})	4670	4840	4770	5060	4250	4260	4560	2860	3270
ρ (skewness) ($\times 10^2$)	169	162	169	174	186	160	194	172	133
λ_{max} (nm) (PSB)	460	446	455	455	505	543	492	577	620
Opsin shift (cm^{-1})	–	–	–	–	2200	3300	2100	4400	5800
ΔH_{rel} (kcal $\cdot$ mol^{-1})	(0)	1.5	3.5	0.7	(0)	32	27	(0)	16
296 K (MeOH/H_2O):									
λ_{max} (nm) (PSB)	443	433	440	434	498	535	481	570	610
Opsin shift (cm^{-1})	–	–	–	–	2500	3800	2300	5100	6600

[a] Oscillator strengths were determined via least-squares regression by using a log-normal distribution function [224] to represent the λ_{max} absorption band [50,51]:

$$\epsilon(\nu) = \epsilon_0 \exp - \left\{ \frac{\ln 2}{(\ln \rho)^2} \left[\ln\left(\frac{(\nu - \nu_0)(\rho^2 - 1)}{\Delta\nu_{FWHM}\rho} + 1 \right) \right]^2 \right\}, \quad \nu > \nu_0 - \left(\frac{\Delta\nu_{FWHM}\rho}{(\rho^2 - 1)} \right); \quad \epsilon(\nu) = 0, \quad \nu \leq \nu_0 - \left(\frac{\Delta\nu_{FWHM}\rho}{(\rho^2 - 1)} \right)$$

where $\epsilon(\nu)$ is the molar absorptivity at wavenumber ν, ν_0 is the wavenumber at maximum absorptivity, ϵ_0 is the molar absorptivity at ν_0, $\Delta\nu_{FWHM}$ is the full-width at half-maximum in wavenumbers and ρ is the skewness. The skewness is a dimensionless parameter which is an indirect measure of the distribution of vibronic activity into higher vibrational modes due to Franck-Condon activity. The oscillator strength is given by:

$$f = 4.319 \cdot 10^{-9} \sqrt{\pi / \ln 2} \times \epsilon_0 \Delta\nu_{FWHM} \left\{ \frac{\rho(\ln \rho)}{(\rho^2 - 1)} \exp\left(\frac{(\ln \rho)^2}{4 \ln 2} \right) \right\}$$

rhodopsin [51] and bacteriorhodopsin [50] and these studies, coupled with an analysis of the two-photon, photocalorimetric and Raman spectra (see below), lead to the following conclusions.

(a) The 9-*cis*-retinal chromophore in solution (EPA, 77K) has the smallest λ_{max} oscillator strength relative to the other isomers: 1.20 (all-*trans*), 1.00 (9-*cis*), 1.03 (11-*cis*), and 1.05 (13-*cis*) (Table I). The effect of conformation is quite different for the opsin bound chromophores. The oscillator strength of the λ_{max} absorption band of I is observed to be anomalously large (1.11) relative to the λ_{max} absorption bands of R (0.98) and B (1.07). This result can only be rationalized by postulating that the counterion (abbreviated as CTN) is not intimately associated with the imine proton in R, B or I. The counterion lies underneath the plane of the chromophore in R and I, and the primary chromophore–counterion electrostatic interactions involve C15–CTN and C13–CTN. These interactions are responsible for the anomalous oscillator strength of I relative to R and B.

(b) Rhodopsin is energetically stabilized relative to isorhodopsin due to both electrostatic interactions and conformational distortion, both favoring stabilization of R. Molecular orbital calculations suggest that rhodopsin chromophore–CTN electrostatic interactions provide an enhanced stabilization of about 2 kcal $\cdot$ mol^{-1} relative to I [51]. Conformational distortion of the 9-*cis* chromophore-lysine system accounts for about 3 kcal $\cdot$ mol^{-1}.

(c) Energy storage in bathorhodopsin is approx. 60% conformational distortion and 40% charge separation. A majority of the chromophore-protein conformational distortion energy involves interaction of the C13($-CH_3$)=C14–C15=N-lysine moiety with nearby (unknown) protein residues.

(d) Strong interactions between the counterion and

the chromophore in R and I will generate weak, but potentially observable, charge transfer bands in the near-infrared. They key predictions are the presence of an observable charge transfer transition at 859 nm (11 640 cm^{-1}) in I and an analogous, but slightly weaker band at 897 nm (11 150 cm^{-1}) in R. Both transitions involve the transfer of an electron from the counterion into low-lying π^* molecular orbitals. To date, however, these transitions have not been reported.

Two-photon electronic spectroscopy

Two-photon spectroscopy inverts the selection rules, and thus the '$^1B_u^{*+}$' state is now nominally forbidden and the '$^1A_g^{*-}$' state is strongly allowed. (The '$^1A_g^{*+}$' state is also allowed, but is normally too high in energy to be observed, due to red-edge one-photon interference.) The application of this technique to the analysis of the isolated and protein-bound visual chromophores has recently been reviewed [44].

Two-photon spectra of all-*trans*-retinol [46], all-*trans*-retinal [45], and the Schiff and protonated Schiff bases of all-*trans*-retinal [58,230] have been analyzed. These spectra indicate that the '$^1A_g^{*-}$' state is the lowest-lying π,π^* state in all of the visual chromophores with the exception of the protonated Schiff bases [58]. This observation is important to analyses of the pigment spectra.

The two-photon absorption spectrum of rhodopsin in the region 370 nm $< \lambda/2 <$ 510 nm yields a single, inhomogeneously broadened band with a maximum at about 440 nm, about 2300 cm^{-1} above the one-photon absorption maximum [44,57,231]. (Note that the two-photon spectra shown in Fig. 4 have been plotted as a function of the combined energy of the two photons and are vertically shifted so that only the maxima are shown.) The two-photon maximum at 440 nm is primarily associated with the '$^1A_g^{*-}$' $\leftarrow S_0$ transition, but the '$^1B_u^{*+}$' state is also two-photon allowed due to initial and final state contributions and contributes to the band contour. Thus the '$^1A_g^{*-}$' state is above the '$^1B_u^{*+}$' state, a level ordering reversal which is only observed upon protonation of the Schiff base [58]. The energy separation observed in rhodopsin is only consistent with a protonated Schiff base in a neutral protein binding site [44,57,231]. Although Raman and FTIR studies had shown prior to the two-photon investigation that the chromophore was bound to the opsin via a protonated Schiff base linkage (see below), the issue of binding site net charge had not been established. Indeed, the popular model for the binding site based on the dihydo chromophore analog studies of Nakanishi, Honig and co-workers [155] predicted two negative counterions, one interacting with the Schiff base proton and a second near C13. The two-photon results indicate that there is only one negative counterion near the positively charged chromophore. Models that accommodate the two-photon [44,57,61,231,331], one-photon (see above) and analog data (subsection III-B) data were independently proposed by Kakitani et al. [175] and Birge et al. [57]. The key prediction is that a single counterion is below the plane of the molecule and has strong electrostatic interactions with carbon atoms C13 and C15, both of which carry partial positive charges (see Fig. 5).

The two-photon double-resonance spectrum of light-adapted bacteriorhodopsin in D_2O at room temperature is shown in Fig. 4 [331]. This spectrum is unique relative to the other two-photon spectra measured for the visual chromophores and pigments [40,44,45,46,57,58,230] in that it exhibits two low-lying band maxima. The lowest energy band maximum at about 560 nm ($\delta \cong 290$ GM) corresponds within experimental error with the one-photon absorption maximum at 568 nm, and is assigned to the '$^1B_u^{*+}$' $\leftarrow S_0$ transition. The higher energy two-photon band at about 488 nm ($\delta \cong 120$ GM) does not correspond to a resolved one-photon feature and is assigned to the '$^1A_g^{*+}$' $\leftarrow S_0$ transition. Not only is it

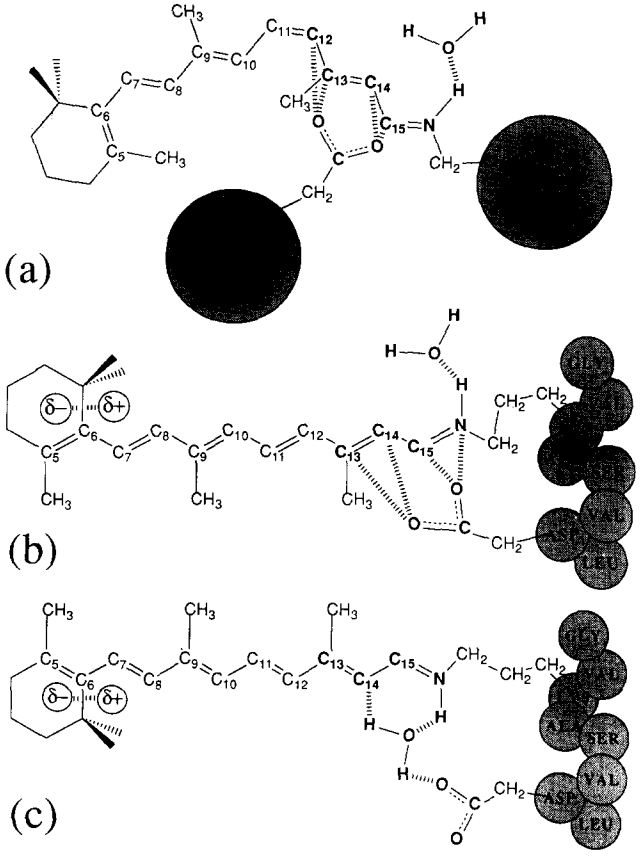

Fig. 5. Possible models of the binding sites of rhodopsin (a) and light-adapted bacteriorhodopsin (b,c). Key electrostatic interactions are indicated with hashed lines. The counterion in rhodopsin is believed to be Glu-113 on helix C near the extracellular surface (see text and Ref. 274). The two models for bacteriorhodopsin are based on the tentative assignment of Asp-212 as the primary counterion, but other polar and/or charged amino acids within the binding site may also interact with the chromophore (see text).

surprising to find that both the '$^1A_g^{*-}$' and '$^1B_u^{*+}$' states generate two-photon maxima, but the observation that the '$^1B_u^{*+}$' state two-photon absorptivity is more than double that associated with the '$^1A_g^{*-}$' state requires special notice. This result indicates that the two-photon absorptivities are dominated by initial and final state contributions (see discussion in Ref. 44), and thus the two-photon absorptivity is proportional to the change in dipole moment upon excitation into the final state. A detailed analysis yields $\Delta\mu$ ('$^1B_u^{*+}$') = 13.5 ± 0.8 D and $\Delta\mu$ ('$^1A_g^{*-}$') = 9.1 ± 4.8 D [331]. The change in the '$^1B_u^{*+}$' state dipole moment determined via two-photon spectroscopy is in good agreement with the field effect measurements of Ponder and Mathies $\Delta\mu$ = 12.4 ± 0.7 D [256].

The recent two-photon measurements on bacteriorhodopsin have not yet been analyzed with respect to the binding site. The results indicate, however, that the binding site of bacteriorhodopsin is very 'ionic' relative to the binding site of rhodopsin. It is thus possible that the binding site carries a net charge (either positive or negative), which add to the degree of difficulty in determining the binding site geometry. In that regard it is worth noting that the recent model proposed by Braiman et al. has three negatively charged groups near the chromophore [68]. This is in sharp contrast to the two-photon results for rhodopsin which indicate a neutral binding site [44,57].

Nuclear magnetic resonance spectroscopy

NMR studies on bacteriorhodopsin have yielded important insights into the geometry of the chromophore in bacteriorhodopsin [58,135–137,201,218,297,298,303]. A key observation of the NMR studies is the fact that the chromophore in rhodopsin is 6-s-*trans* [136], whereas the visual chromophores in solution [39,47] and in vertebrate opsin [297] are 6-s-*cis*. Although previous spectroscopic studies had suggested the possibility that the chromophore in bacteriorhodopsin was unusually planar [278,279], the observation of a 6-s-*trans* chromophore was quite unexpected. Previous NMR experimental [158] and a number of theoretical [47,158,159] investigations suggest that the 6-s-*trans* conformation in the retinal isomers is about 4 kcal · mol^{-1} higher in energy than the 6-s-*cis* conformation (see Fig. 4 of Ref. [47]). NMR studies have also provided direct evidence for proton exchange between the bacteriorhodopsin Schiff base and bulk water [135].

De Groot et al. have carried out a high-resolution, solid-state ^{15}N-NMR investigation of the Schiff base environment in bacteriorhodopsin [80]. Based on comparisons with model compound chemical shift anisotropies, these authors conclude that the counterion environment is complex and may involve several neutral protic species or may involve a water-mediated aspartic acid residue. The key observation is that a single aspartic acid or tyrosinate residue hydrogen bonded to the Schiff base proton is not compatible with the NMR data.

Resonance Raman spectroscopy

Resonance Raman spectroscopic studies have contributed more to our understanding of the geometry of the protein-bound chromophores than any other spectroscopic investigations. The pioneering investigations of Mathies and co-workers [33,67,110,112,219,221,249, 300,301,302] and Callender and co-workers [17,18,72, 73,83,246,250] provided some of the key preliminary analyses of chromophore geometry. Subsequently, a collaboration between Lugtenberg and Mathies has provided definitive vibrational assignments for the resonane Raman spectra of both the isolated and protein-bound chromophores, through the synthesis and spectroscopic analysis of a large collection of deuterated and ^{13}C isomers [221,300,301,302]. More recently, time-resolved resonance Raman techniques have provided in-

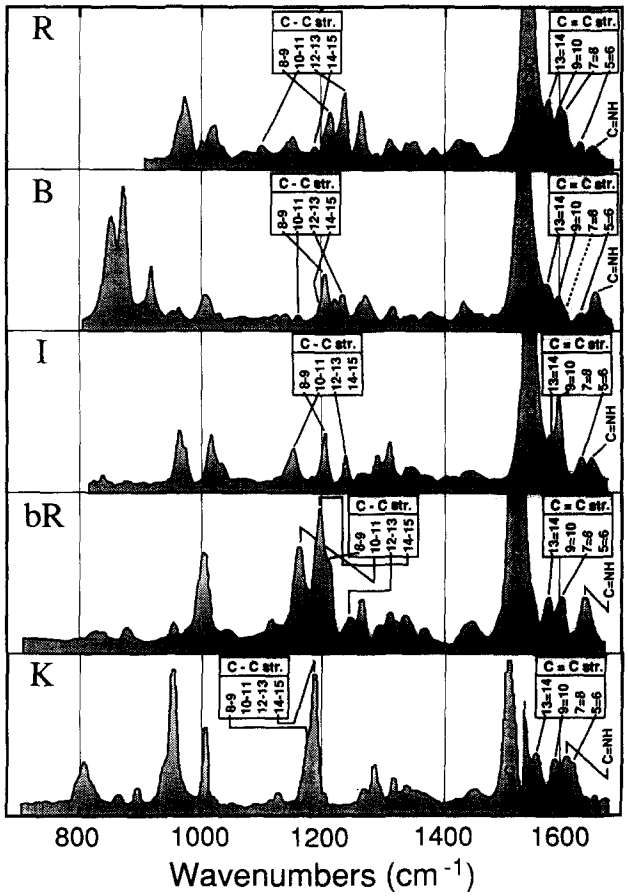

Fig. 6. Resonance Raman spectra of rhodopsin (R), bathorhodopsin (B), isorhodopsin (I), light adapted bacteriorhodopsin (bR) and K. Approximate vibrational assignments are indicated based on the analyses discussed in this review and presented in Table II. The spectra of R, B and I were provided in digital form by Prof. R.H. Callender and the spectra of bR and K were digitized from spectra provided by Prof. R.A. Mathies.

TABLE II

Selected literature vibrational assignments and observed frequencies (cm^{-1}) for the all-trans, 9-cis, 11-cis and 13-cis protonated Schiff bases and for the corresponding vertebrate and bacterial opsin pigments

Data are compiled from Refs. 18, 24, 25, 82, 100, 221, 249, 250, 266, 267, 270, 271, 295, 296, 300, 301, 304. When literature assignments differed, averages of the literature values are reported. Relative Raman line intensities are listed in parentheses (s = strong, m = medium, w = weak).

Mode [a]	11-*cis*		all-*trans*			9-*cis*		13-*cis*	
	PSB	R	PSB	B	bR	PSB	I	PSB	K
C15=NH Str	1658 (w)	1.657 (w)	1657 (w)	1655 (w)	1640 (w)	1659 (w)	1655 (w)	1656 (w)	1609 (w)
C15=ND Str	–	1624 (w)	1632 (w)	1625 (w)	1624 (w)	–	1631 (w)	–	1575 (w)
ND Shift	–	33	26	31	16	–	24	–	34
C8–C9 Str	1217 (s)	1217 (s)	1194 (s)	1214 (s)	1214 (m)	1204 (s)	1206 (s)	1202 (s)	1187 (m)
C10–C11 Str	1093 (w)	1098 (w)	1159 (m)	1166 (w)	1170 (m)	1137 (m)	1154 (s)	1166 (m)	–
C12–C13 Str	1237 (s)	1239 (s)	1237 (w)	1240 (m)	1255 (w)	1238 (m)	1242 (s)	1226 (w)	–
C14–C15 Str	1190 (w)	1190 (w)	1191 (w)	1210 (w)	1201 (s)	1189 (s)	–	1176 (w)	1195 (s)
$[C=C]_{sym}$ Str	1556 (s)	1547 (s)	1563 (s)	1536 (s)	1527(s)	1567 (s)	1549 (s)	1565 (s)	1517 (s)
C13=C14 Str	–	1581 (m)	–	1578 (w)	1581 (w)	–	1585 (w)	–	1560 (w)
C9=C10 Str	–	1599 (m)	1596 (w)	1595 (w)	–	–	1599 (m)	1595 (w)	1590 (w)
C7=C8 Str	–	1608 (w)	–	–	1600 (w)	–	–	–	–
C5=C6 Str	–	1636 (w)	1612 (w)	1629 (w)	–	–	1636 (w)	–	1618 (w)

[a] Modes are defined based on the principal C–C, C=C or C=N stretching (Str) normal mode eigenvectors. In most cases, other stretching and binding modes contribute to the vibrational band in significant proportion (see Refs. 82, 296, 301). Accordingly, these assignments are very approximate and are used primarily for labelling convenience (see text). The abbreviation '$[C=C]_{sym}$ Str' refers to the strongly Raman active mode, or collection of overlapping modes, involving primarily in phase (symmetric) stretching motions of C7=C8, C9=C10, and C11=C12 bonds.

sight into the molecular changes accompanying the formation of the early intermediates [10,16,86,106,120, 131,134,160,307,317]. A number of excellent reviews are available [73,219,221] and this discussion will concentrate on those assignments particularly relevant to an analysis of chromophore–protein interactions as well as the conformational changes accompanying the primary event.

The Raman spectra of rhodopsin (R), isorhodopsin (I), bacteriorhodopsin (bR) and their primary photoproducts (B and K) are shown in Fig. 6, and selected vibrational assignments based in large part on the Raman data are presented in Table II. The Raman studies have resulted in the following key observations for bacteriorhodopsin:

(a) The Schiff base is protonated in all of the pigments and their primary photoproducts [9,10,67,83,86, 160,214,219,221,295,300,307,309,317].

(b) The imine proton is strongly hydrogen bonded in bR and L, but is in a significantly different environment in K [10,86,221,295].

(c) There is evidence for one or more water molecules near, or hydrogen bonding to, the imine proton in bR [147].

(d) The geometry of the C14–C15 bond is s-*trans* and the C15=N bond is *trans* in all of the light-adapted species investigated [112,113]. This is a controversial finding as it applies to K and L, because the popular model proposed by Tavan and Schulten for the primary event predicts that the primary photochemistry is bR (13-*trans*, 14-s-*trans*, 15-*trans*) to K (13-*cis*, 14-s-*cis*, 15-*trans*) followed by a thermal reaction to L (13-*cis*, 14-s-*cis*, 15-*trans*) [280,281,314,315,316]. Clearly, if the analyses of Smith et al. are correct, the key elements of the Tavan and Schulten model are incorrect. The debate centers on the interpretation of the fingerprint vibrations, and as of this review, the issue remains unresolved. The reader is referred to the recent articles by Fodor et al. [113] and Tavan and Schulten [315] for a discussion of both sides. We will discuss this interesting issue from a different perspective below.

Fourier transform infra-red spectroscopy

FTIR spectroscopy provides a different perspective on the binding site than that provided by resonance Raman spectroscopy. The key difference is associated with the fact that the vibrational transitions observed by using resonance Raman spectroscopy are associated solely with the chromophore whereas FTIR difference methods observe vibrational modes associated with both the chromophore and the protein, provided the modes differ between the two protein states. While one might also anticipate that the difference in selection rules between infrared absorption and Raman scattering would also generate differences, as noted by Rothschild et al., the active chromophore vibrations are very similar in both techniques [268]. This result is due to the lack of symmetry of the chromophore/protein. Nevertheless, the two techniques are complementary because of the different selectivity.

FTIR spectroscopy has been applied with great success in evaluating the binding sites of both rhodopsin [24,69,81,121,233,267,275,294] and bacteriorhodopsin [3,68,69,90,99,105,233,260–262,265,266,268,269,271, 275,293].

Some of the more interesting observations derived from FTIR studies involve the secondary amino acid changes during the photocycle of bacteriorhodopsin. The key changes involve tyrosine and aspartic acid changes [68,90,91,107,260,261,269]. The following represents a recent model of Braiman et al. based on FTIR studies of mutants [68]:

bR	[Asp-85 (COO^-);	Asp-96 (COOH);	Asp-115 (COOH);	Asp-212 (COO^-);	Tyr-185 -O^-]
K	[Asp-85 (COO^-);	Asp-96 (COOH);	Asp-115 (COOH);	Asp-212 (COO^-);	Tyr-185 -OH],
L	[Asp-85 (COO^-);	Asp-96 (COO^-);	Asp-115 (COOH);	Asp-212 (COO^-);	Tyr-185 -OH],
M	[Asp-85 (COOH);	Asp-96 (COOH);	Asp-115 (COOH);	Asp-212 (COOH);	Tyr-185 -O^-].

FTIR studies have also provided evidence that the polyene chain of the chromophore in bacteriorhodopsin lies roughly perpendicular to the membrane plane [99]. (The chromophore shown in Fig. 2 was rotated into the membrane plane to show more clearly the polyene chain and β-ionylidene ring.) The recent reviews by Braiman [69] and Rothschild [266] are recommended.

Time-resolved optical spectroscopy

The primary photochemical events in both rhodopsin and bacteriorhodopsin generate bathochromically shifted photoproducts on a picosecond time scale. The intermediates that are formed during the subsequent dark reactions each have well-defined optical absorption spectra. Thus, time-resolved optical spectroscopy represents a key spectroscopic tool for analyzing the kinetics associated with the primary events as well as the subsequent dark reactions [8,71,85,89,93,123,129, 148,167,170,183,220,222,229,238,252–255,283,284,292].

Time-resolved studies on rhodopsin indicate that bathorhodopsin can be formed from either rhodopsin or isorhodopsin within about 3 ps [8,71,93,129,167,229, 292]:

$$\underset{(11\text{-}cis)}{\text{rhodopsin}} \xrightarrow{\sim 3\ \text{ps}} \underset{(\text{all-}trans)}{\text{bathorhodopsin}} \xleftarrow{\sim 3\ \text{ps}} \underset{(9\text{-}cis)}{\text{isorhodopsin}}$$

Because it is known that rhodopsin contains an 11-*cis* chromophore, that isorhodopsin contains a 9-*cis* chromophore and that the bathorhodopsin products are identical, these observations indicate that chromophore isomerization occurs in picoseconds. We will demonstrate below that this observation requires a barrier-less excited state potential surface.

Most of the recent time-resolved experiments have been carried out on bacteriorhodopsin [14,15,89,123, 170,183,220,238,252,253,255,283,284]. These experiments indicate the formation of a precursor to K, called J, which is believed by most researchers to be a ground state species with a 13-cisoid structure [89,220,253,255]:

$$\text{bR} \xrightarrow{\sim 0.5\ \text{ps}} \text{J} \xrightarrow{\sim 5\ \text{ps}} \text{K}$$

The differential absorption changes accompanying the primary photochemical event in bacteriorhodopsin are shown in Fig. 7 [220]. The possibility that J might be a mixture of ground and trapped excited state species has been proposed based on theoretical calculations [53]. This controversial position will be discussed in greater detail below.

Time resolved spectroscopy on a slower time scale has also been carried out to investigate the number of intermediates in the photocycle of bacteriorhodopsin [327]. These studies indicate that at least six distinct intermediates are formed after K under the assumption of first-order kinetics. The authors note, however, that the photocycle of bacteriorhodopsin may exhibit distributed kinetics, and thus the above number of intermediates may require revision [327].

III-B. Chromophore analog and site-directed mutagenesis studies

Two methods of studying the binding sites of rhodopsin and bacteriorhodopsin deserve special notice, because they have provided unique insights into the binding sites of both proteins. Chromophore analogs,

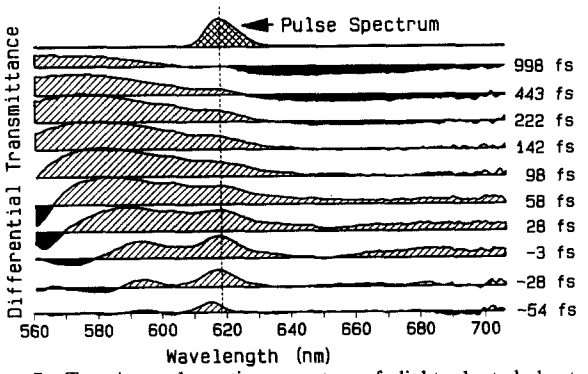

Fig. 7. Transient absorption spectra of light-adapted bacteriorhodopsin as a function of delay time in femtoseconds (1 fs = 10^{-15} s). The pump pulse at 618 nm (dashed line) had a duration of 60 fs, and the delayed probe pulses were 6 fs in duration. (Reproduced with permission from Ref. 220).

when incorporated into the binding site, provide a method of examining the nature of the protein chromophore interactions as well as geometry of the chromophore. Site-directed mutagenesis provides a method of examining the importance of individual amino acids on the structure and function of the protein. This section evaluates the contribution both methods have made to our understanding of the chromophore binding sites of rhodopsin and bacteriorhodopsin.

Chromophore analog studies

During the past decade, hundreds of chromophore analogs have been incorporated into the binding sites of rhodopsin and bacteriorhodopsin, and the observation of the resulting opsin shifts and/or photochemical characteristics have been analyzed in terms of chromophore-protein electrostatic and conformationally restrictive interactions [5,7,12,13,20–23,29,34,57,72,77,81, 84,91,105,111,113,115,116,136,137,155,180,196,197,198, 198,199,200,201,202,210,212,221,234,259,271,278,279, 285–288,297,299,300,302,306,320,321]. The opsin shifts for selected chromophore analogs incorporated into bacterio-opsin, vertebrate opsin and *Chlamydomonas* opsin are presented in Fig. 8. The analogs will be identified in our discussion by reference to the boldface number that appears inside the β-ionylidene ring. The following observations have been made based on analog studied:

(1) Locked 11-*cis* analogs (5 and 6) yield a pigment which will not generate bathorhodopsin upon excitation [5,57,71,84]. These observations indicate that the primary photochemical event in vertebrate rhodopsin involves an 11-*cis* to 11-*trans* photoisomerization. Because these analogs block formation of metarhodopsin

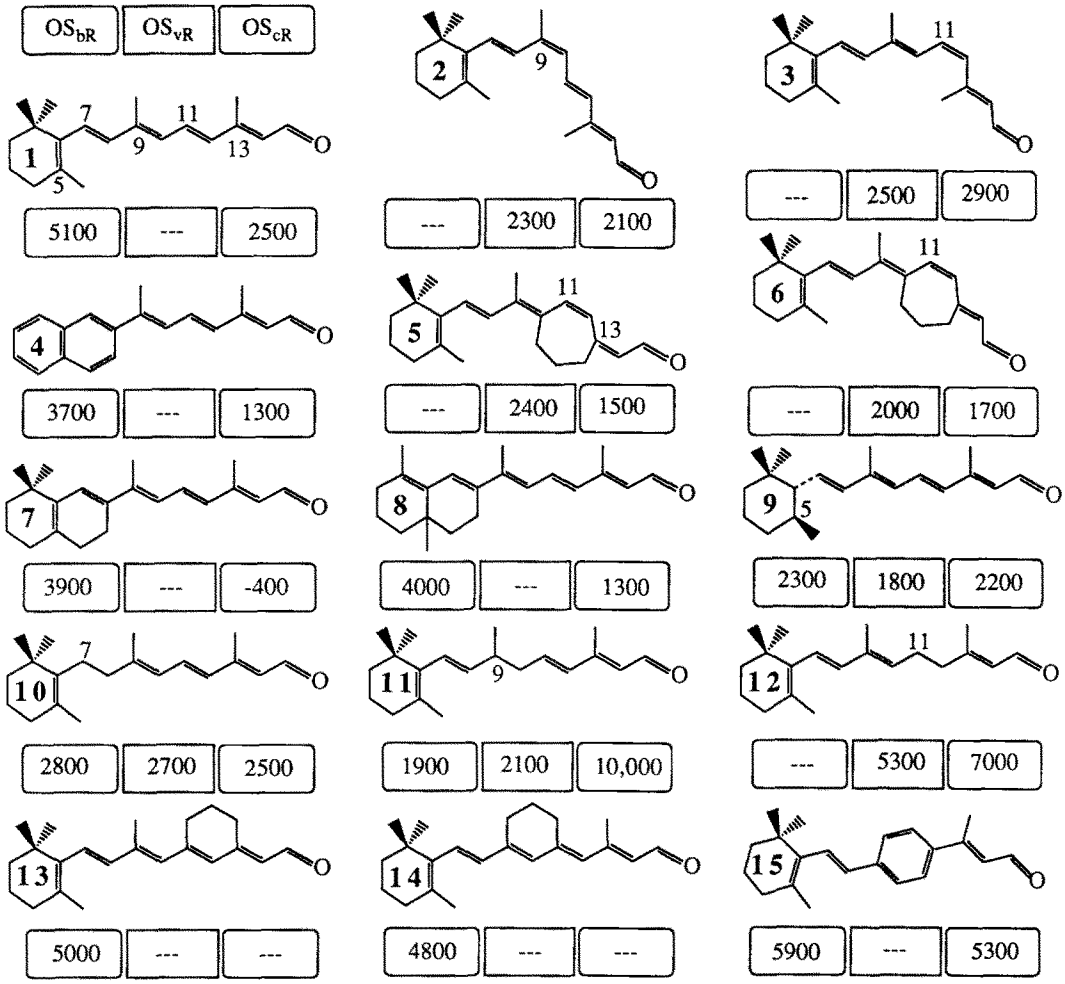

Fig. 8. Opsin shifts associated with the incorporation of chromophore analogs into *Halobacterium halobium* (bacterio) opsin (OS$_{bR}$), bovine (vertebrate) opsin (OS$_{vR}$) and *Chlamydomonas reinhardtii* opsin (OS$_{cR}$). All shifts are given in wavenumbers and are relative to the protonated Schiff base in methanol. For example, the absorption maximum of the chloride salt of the *n*-butylamine protonated Schiff base of all-*trans*-retinal (1) in methanol is 440 nm (22700 cm^{-1}). The absorption maximum of the pigment formed when all-*trans*-retinal is incorporated into bacterio-opsin is 568 nm (17600 cm^{-1}). The opsin shift is therefore 22700 − 17600 = 5100 cm^{-1}. Uncertainties in band maxima assignments due to inhomogeneous broadening yield opsin shift uncertainties of ±300 cm^{-1}. The data are taken from Table I and Refs. 12, 29, 114, 115, 155, 234, 252, 305, 306.

II, and the formation of this intermediate is required to activate transducin [127,203], we conclude that isomerization is required for the activation of vertebrate rhodopsin.

(2) Similarly, bacteriorhodopsin pigments generated with locked 13-*cis* analogs do not pump protons, suggesting that isomerization is also required for bR activity [180].

(3) All of the analogs that could be incorporated into *Chlamydomonas* opsin (1–12,15)-generated active pigments [114,115]. Either chromophore isomerization is not required to activate *C. reinhardtii* or photoisomerization about the terminal C=N bond is a potential activation mechanism that operates in the absence of alternative isomerizations (such as 11-*cis* → 11-*trans*).

(4) Spectroscopic studies of analogs 7 and 8 incorporated into bacteriorhodopsin [320] supports the NMR study predicting that the native protein contains a 6-s-*trans* chromophore [136]. In particular, 8 rapidly generates a pigment with an absorption maximum at 564 nm, undergoes light-dark adaptation, and has a proton pump efficiency of about 90% [320]. In contrast, 7 slowly generates a pigment with an absorption maximum at 596 nm, does not undergo light-dark adaptation and has a proton pump efficiency of about 20%. The observation that 7 and 8 have very similar opsin shifts, however, would seem to argue against a salt bridge in close proximity to the β-ionylidene ring unless the negative charge is placed directly above (or below) the center of the ring.

(5) A study of the di-hydro analogs (9–12) incorporated into vertebrate opsin generated the well-known external point charge model of the rhodopsin binding site [12,155]. This model proposed two negatively charged counterions near the chromophore, one associated with the Schiff base proton and the second near C13. Subsequent two-photon studies indicated, however, that there is only one negative counterion near the positively charged chromophore [44,57,61,231]. The model shown in Fig. 5 accommodates both the one-photon and two-photon data [51,57,175].

(6) Incorporation of the 9-*cis* isomer of the 5,6-dihydro chromophore (9) into bovine opsin yields an isorhodopsin pigment analog ($\lambda_{max} = 461$ nm) with unusual photochemical properties [6,329]. Photolysis of 5,6-diH-isorhodopsin at ambient temperature generates a blue-shifted photoproduct (called BSI, $\lambda_{max} = 430$ nm) [6], bypassing the formation of the primary batho photoproduct ($\lambda_{max} = 508$ nm) which is stable below 31 K [329]. This observation suggests that a major relaxation mode in bathorhodopsin involves the β-ionylidene ring. Recent studies by Kliger and co-workers on rhodopsin and isorhodopsin indicate that there is a blue-shifted photoproduct between batho and lumi in the native protein photobleaching sequence [102,165, 191].

(7) Di-hydro analogs (9–11) have also been incorporated into bacteriorhodopsin [234] and sensory rhodopsin [306]. A point charge model with a negative charge about 4 Å from the Schiff base proton, a negative charge near C_5 and a positive charge above the β-ionylidene ring near C_1 and C_2 [306]. While this model accommodates the dihydro data, the placement of charges near the ring does not accommodate the opsin shift data for 7 and 8. The model for bR in Fig. 5 accommodates the opsin shifts for both data sets.

(8) The viability of models involving adjacent (C10–C11) single bond rotations during the primary event of rhodopsin [198,202] was studied by Sheves and co-workers [286]. These investigators demonstrated that an artificial visual pigment with restricted C9–C11 dihedral motion generated normal photolysis intermediates indicating that rotation about the C10–C11 bond does not take place.

The above examples are selective and represent but a small fraction of the analog studies that have been carried out. For detailed discussions of other analog studies see Refs. [29,84,285].

Site-directed mutagenesis studies

Site-directed mutagenesis (SDM) provides one of the most powerful tools for investigating structure–function relationships in proteins. Although some investigations of rhodopsin have been reported (see below), the majority of work in this area has concentrated on bacteriorhodopsin [3,35,63,68,70,98,133,178,227,228,265]. Through the selective replacement of individual amino acids within bacterioopsin, it is in principal possible to determine the role that each amino acid plays in translocating protons. The major problem that generates ambiguity is the possibility that the protein can modify its tertiary structure to accommodate the loss of a key amino acid, and in the process mask the relevance of the replaced amino acid in the structure-function scheme. It is also often difficult to differentiate between structurally important amino acids versus mechanistically important amino acids. Thus, an amino acid that upon replacement dramatically diminishes the proton pumping ability of bacteriorhodopsin may be a crucial component of the proton conduction/pumping system or be a crucial mediator of tertiary structure. Analysis of SDS results must be tempered by such considerations.

There is no general agreement in the literature with regard to assignment of the primary counterion in bacteriorhodopsin. While our models have assigned Asp-212 as the primary counterion [50,52,53,60,331] (e.g., Fig. 5), other studies have suggested that Tyr-185 is the primary counterion [261,269]. The possibility that there are three negatively charged groups near the chromophore (Asp-85, Tyr-185 and Asp-212) with the two Asp groups mediated by a positively charged Arg-82 has also been

proposed [68]. Khorana and co-workers [133,228] have investigated the effect of individual replacements of each of the above-mentioned amino aicds, as well as other potential counterion candidates, and the results are summarized in Table III. From these data it appears that Asp-212 is the most likely candidate for the primary counterion in light adapted bacteriorhodopsin because the replacement of Asp-212 with Ala generates a light unstable pigment with a 50-fold longer regeneration time. The fact that this replacement can still generate a light stable dark adapted species suggests that the counterion in the 13-*cis* dark-adapted species differs from that in the all-*trans* light-adapted species. These studies also provide evidence that Asp-85, Asp-96, Asp-212 and Tyr-185 are involved in the proton-conduction mechanism [133,228]. The above discussion on FTIR provides further details on this issue.

A recent SDM study by Sakmar et al. indicates that Glu-113 is the primary counterion in bovine rhodopsin [274]. Whereas substitution of Glu-122 and Glu-134 with uncharged amino acids generates only modest spectroscopic shifts, substitution of Glu-113 by Gln-113 generates a blue shifted pigment with $\lambda_{max} = 380$ nm. This result suggests that there is only one counterion near the chromophore, and provides support for the neutral binding site model predicted by two-photon spectroscopy [57].

III-C. The binding site of rhodopsin

The above studies yield the binding site model shown in the top of Fig. 5. The purpose of this section is to briefly overview the key features of this model. Two-photon studies indicate that the binding site is neutral [44,57,231], and hence there is only one negatively charged counterion in the vicinity of the chromophore. An analysis of the primary structure (Fig. 1) indicates that the most likely candidates are Asp-83 (B helix), Glu-113 (C helix), Glu-122 (C helix) and Glu-134 (C helix). Presumption of a similarity of the rhodopsin tertiary structure with that observed for bR (Fig. 2) suggests that one of the glutamic acid residues on helix C is the primary counterion. Site-directed mutagenesis studies indicate that Glu-113 is the most likely candidate [274]. Raman, FTIR, one-photon, two-photon, photocalorimetric and chromophore analog studies are consistent with the model shown in Fig. 5 [51,57,175].

TABLE III

Site specific mutagenesis investigations of substitutions of potential chromophore counterions in dark-adapted and light-adapted bacteriorhodopsin

All data are from Refs. 133, 227, 228.

No.[a]	Native [b]	Mutant [b]	$t_{1/2}^{Reg}$ [c] (min)	Reg [d] (%)	λ_{max}^{DA} [e] (nm)	λ_{max}^{LA} [f] (nm)	$k_{init.}^{H^+}$ [g] ($bR^{-1} \cdot s^{-1}$)	$\Lambda_{SS}^{H^+}$ [h] (bR^{-1})
36 Cyt	Asp	Asn	1.3	60	550	560	3.9	56
38 Cyt	Asp	Asn	1.3	72	553	563	3.6	58
85 C	Asp	Asn	20	34	587	594	n.d. [i]	n.d.
85 C	Asp	Glu	< 0.1	57	556	560	1.1	20
96 C	Asp	Asn	2.3	73	553	560	0.1	3
96 C	Asp	Glu	1.2	72	553	561	2.8	47
102 Cyt	Asp	Asn	1.1	72	553	563	3.3	47
104 Cyt	Asp	Asn	2.1	76	550	560	3.5	48
115 D	Asp	Asn	6.0	42	545	544	1.9	40
115 D	Asp	Glu	4.6	34	541	543	1.1	20
185 F	Tyr	Phe	8.7	–	540	570	0.8	13
194 F	Glu	Gln	2.0	–	541	545	1.0	16
212 G	Asp	Asn	31	64	560	548	0.5	6
212 G	Asp	Glu	38	57	584	581	0.2	2
212 G	Asp	Ala	50	51	540	l.u. [j]	l.u.	l.u.

[a] Amino acid number and putative helix assignment (see Fig. 1).
[b] The amino acid in the native protein is listed under the column labelled 'Native' and the amino acid replacing it in the mutated protein is listed under the column labelled 'Mutant'.
[c] Half-time in minutes for regeneration of the mutant opsin with all-*trans*-retinal to form the chromophore-protein complex.
[d] Percent of protein regeneration based on all-*trans*-retinal incorporation.
[e] Long-wavelength absorption maximum of dark-adapted protein (nanometers).
[f] Long-wavelength absorption maximum of light-adapted protein (nanometers).
[g] Initial rate of proton pumping (protons/bR per s).
[h] Steady state extent of proton pumping (protons/bR).
[i] n.d., not detected.
[j] l.u., light unstable.

Models which move the counterion one or two atoms closer to the center of the polyene chain and simultaneously closer to the polyene atoms are also possible. However, the positive charge is primarily localized on atoms C13, C15 and the imine proton [54,58], and one oxygen atom must be within about 4 Å of this section in order to accommodate the transition energy and oscillator strength data [51].

One or more water molecules are present within the binding site [257], and the observation of an ND shift of 33 cm^{-1} (Table II) suggests that one water molecule is hydrogen bonded to the imine proton (Fig. 5). This is a somewhat controversial assignment, because many investigators assume that the imine proton is hydrogen bonded to a negatively charged counterion based on deuterium isotope effects. It is generally recognized that a large $\nu_{C=N}$ deuterium (ND shift) isotope shift is characteristic of strong hydrogen bonding to the imine proton [24,82,249]. Based on this argument, hydrogen bonding is strongest in R (ND shift $\approx$ 33 cm^{-1}), strong in B (ND shift $\approx$ 31 cm^{-1}) and moderately strong in I (ND shift $\approx$ 24 cm^{-1}) (Table II). As comparison, the all-*trans* protonated Schiff base (ATRPSB) in methanol exhibits a ND shift of about 26 cm^{-1}. Spectroscopic studies of ATRPSB indicate that the counterion is intimately associated with the imine proton in non-polar environments [58]. The work of Blatz [64] suggests that in highly polar, strongly hydrogen bonding solvents, the counterion is highly solvated and the imine proton is hydrogen bonded with the solvent. The ND shift has been measured for ATRPSB in both environments and differs by only 3 cm^{-1} [82,249,301]. One concludes that the ND shift, while diagnostic of hydrogen bonding, is not sensitive to the *nature* of the hydrogen bond. A quantitative relationship between the ND shift and the strength of a hydrogen bond to the imine proton has not been firmly established (for more details see Refs. 82, 174, 206, 207).

Although the ND shift is largest in R, it drops by only 2 cm^{-1} in going from R to B. This difference is anomalously small for an isomerization moving the $-C_{15}$=NH- moiety away from a fixed counterion. Any attempt to maintain a strong hydrogen bond between the imine proton and the counterion following a one-bond 11-*cis* $\rightarrow$ 11-*trans* photoisomerization will fail to accommodate the observed oscillator strength and spectral shifts.

Many proponents of hydrogen bonding between the counterion and the imine proton in R suggest that the imine proton is hydrogen bonded to an uncharged protein residue in B. This model accommodates the bathochromic shift, but does not explain adequately the remarkable similarity of $\nu_{C=NH}$ and $\nu_{C=ND}$ in R, B and I (Table II). One concludes, based on the force field calculations of Deng and Callender [82], and the model compound studies of Baasov et al. [19,20,22], that $\nu_{C=NH}$ and $\nu_{C=ND}$ are rather sensitive to the charge on the hydrogen bonding species. The above model is also incapable of rationalizing a weaker hydrogen bond to the counterion along with a blue shifted absorption maximum in I. Hydrogen bonding of the imine proton to water provides the best model, because it explains both the magnitude and the similarity in the ND shift observed in R, B and I. We conclude that Fig. 5 provides the most realistic model for the binding site in rhodopsin.

III-D. The binding site of bacteriorhodopsin

The nature of the bacteriorhodopsin binding site remains a subject of intense study and only modest agreement. Two possibilities are presented in Fig. 5 based on the assumption that Asp-212 is the primary counterion. While it is known that the polyene chain of the chromophore lies perpendicular to the membrane plane [99], the orientation of the NH bond is not known with certainty. The orientation shown in Fig. 5b will move the imine proton in the direction of the proton pumping upon 13-*trans* to 13-*cis* photoisomerization. While this assignment is intuitively pleasing, recent neutron diffraction [145,146] and linear dichroism [194] studies suggest the inverted orientation shown in Fig. 5c. To complicate this issue further, time-resolved photoinduced voltage measurements on oriented bacteriorhodopsin indicate that positive charge is moved in a direction opposite to that of the ultimate proton pumping direction [132,150,177,245,318]. This observation might upon first inspection be interpreted to indicate that the Schiff base proton moves in the opposite direction during the bR $\rightarrow$ K step versus in the L $\rightarrow$ M proton release step. If this interpretation is correct, it would favor the oritentation shown in Fig. 5c. However, if the primary event is a one-bond 13-*trans* $\rightarrow$ 13-*cis* photoisomerization, and if the β-ionylidene ring remains fixed during the primary event, net motion of the Schiff base proton during this transformation is minor. Most of the charge translocation involves motion of C15, which carries a position charge of about 0.25. A close examination of Fig. 5 indicates that a 13-*trans* $\rightarrow$ 13-*cis* photoisomerization of the chromophore in Fig. 5b would generate charge migration in an opposite sense to the net proton pumping. In contrast, a 13-*trans* $\rightarrow$ 13-*cis* photoisomerization of the chromophore in Fig. 5c would generate charge migration in the same direction as the net proton pumping. Thus, in the absence of contrary motions by polar protein residues during the primary event, the above analysis would appear to support the orientation shown in Fig. 5b. The above conflicting observations preclude a definitive orientation assignment, and thus Figs. 5b and 5c are included to emphasize the uncertainty. While there is evidence for charged perturbations near the β-ionyli-

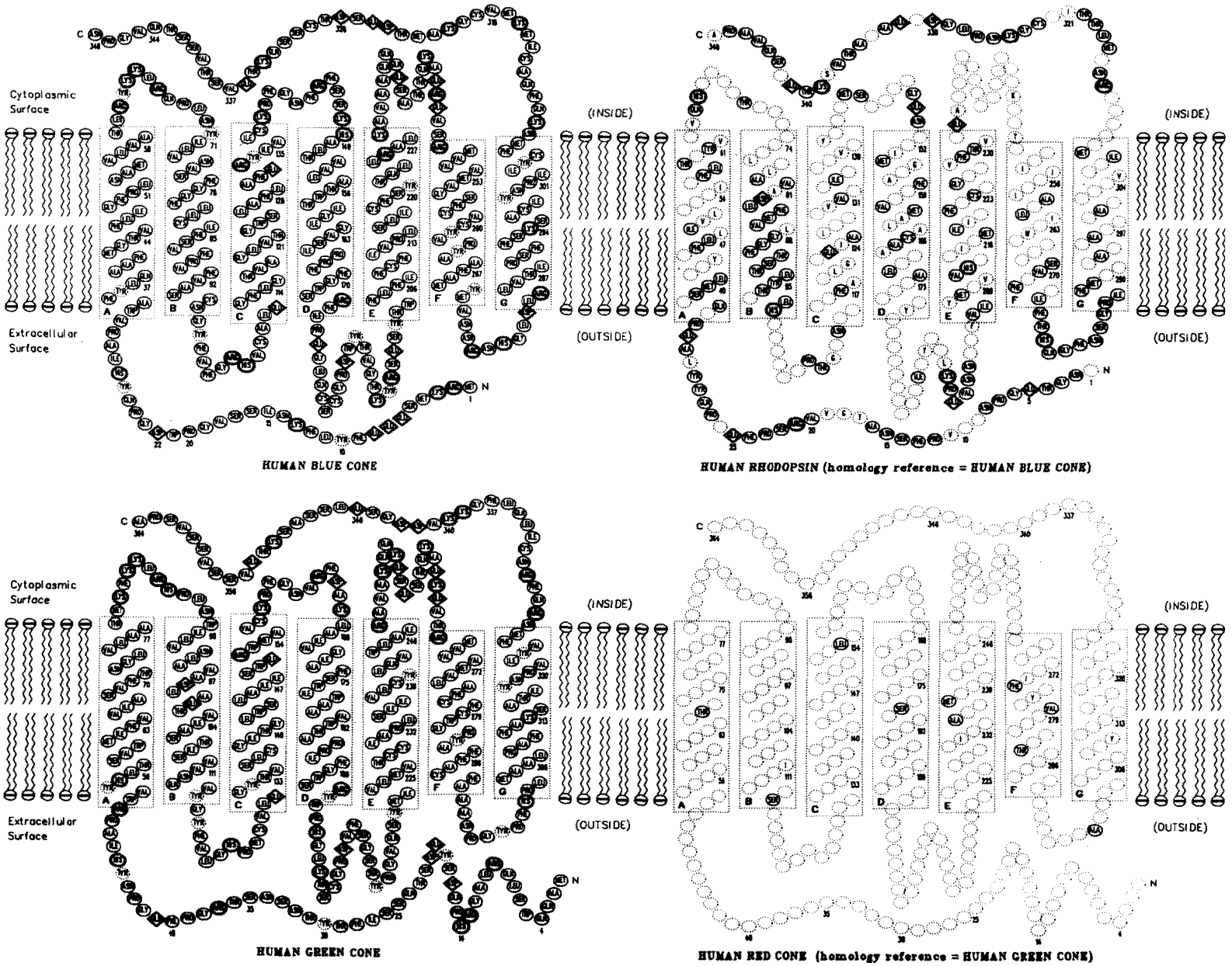

Fig. 9. Amino acid sequences and putative membrane spanning regions of human blue cone (upper left) and human green cone (lower left). The diagram at upper right examines the homology between the blue cone and human rhodopsin. The diagram at lower right examines the homology between the green cone and the red cone. Only those amino acids which differ from those found in the protein on the left are indicated. One-letter and three-letter codes are used following the homology distinctions outlined in the caption to Fig. 1.

dene ring [80,136,298], the nature of the charges, or the possibility that a dipolar group is responsible, remains an open question. Third, the two-photon measurements suggest that the binding site may be charged, and hence there may be more than one counterion in the vicinity of the chromophore. Recent NMR studies confirm the complexity of the counterion environment [80].

III-E. The binding sites of the human cone pigments

The amino acid sequences and putative membrane spanning regions of the human cones are shown in Fig. 9 displays the homology between the blue cone and human rhodopsin. The diagram at lower right of Fig. 9 displays the homology between the green cone and the red cone. Knowledge of the primary structure of the cone pigments offers a significant opportunity to probe the molecular origins of wavelength regulation in the visual pigments. Unfortunately, few studies have been carried out on the cone pigments, and we present this section largely to stimulate further work in this area. For convenience, we will use rhodopsin sequence numbers to refer to individual amino acids, but as shown in Fig. 9, the transmembrane assignments for the cone pigments differ for homologous amino acids.

The blue cone has significant homological overlap with rhodopsin and is particularly interesting to study because two of the potential counterions in rhodopsin (Asp-83 and Glu-122) are replaced with neutral amino acids (see Fig. 9). However, the amino acid assigned via SMD to be the primary counterion (Glu-113) is conserved in the blue, red and green cone opsins. Thus, if the Glu-113 primary counterion assignment is correct, wavelength regulation in the cone pigments could potentially involve altering the geometry of the chromophore counterion interaction. The following study, however, suggests that in the blue cone pigment a change in the primary counterion may be involved in wavelength regulation.

A recent resonance Raman study has demonstrated that the 440 nm cone pigment of the toad (*Bufo marinus*) contains a protonated Schiff base chromophore lacking a counterion interaction near the center of the polyene chain [208]. This conclusion might appear to conflict with the observation that Glu-113 is conserved. However, it is possible that the binding site is modified in the blue pigment to prevent nearest neighbor interactions between the chromophore and Glu-113. However, the total removal of all counterions from the vicinity of the protonated Schiff base chromophore would generate a red shifted ($\lambda_{max} \approx 600$ nm) rather than a blue shifted chromophore, and hence the observation of no chromophore–counterion interactions near the center of the polyene provides only one part of the answer. What remains to be explained is what amino acid provides the new counterion, and why does this counterion blue shift the absorption maximum relative to the primary counterion? It is possible that Tyr-262 (or Tyr-265) on helix F (Fig. 9) provides the primary counterion in the blue cone and the loss of the counterion near the center of the polyene chain induces tyrosine → tyrosinate formation in order to stabilize the protonated Schiff base. This interaction would take place closer to the C15=NH linkage (where most of the positive charge is localized [54]) and shift the absorption band to shorter wavelengths through more effective electrostatic stabilization of the ground state.

IV. The primary photochemical event in rhodopsin

There remains uncertainty with respect to the assignment of the true 'primary' photoproduct. There are three candidates: photorhodopsin ($\lambda_{max} \cong 560$ nm), hypsorhodopsin ($\lambda_{max} \cong 435$ nm) and bathorhodopsin ($\lambda_{max} \cong 530$ nm). There is now a general consensus that hypsorhodopsin is an artifact generated via multiphoton processes [290,329]. The question that remains to be answered is whether bathorhodopsin has a ground state precursor, photorhodopsin. Recent picosecond experiments suggest that there is a ground state intermediate (photorhodopsin) that forms prior to bathorhodopsin, and that bathorhodopsin (in cattle) has a formation time on the order of about 40 ps [290,329]. Early picosecond experiments indicated that 'bathorhodopsin' forms in about 3 ps [229,251], and that this same photoproduct could also be formed from isorhodopsin in about 3 ps [229]. These experiments attributed the first bathochromically shifted absorption band to 'bathorhodopsin', and thus these studies may have been observing photorhodopsin rather than bathorhodopsin. However, photorhodopsin cannot be trapped at low temperatures, and therein lies an interesting dilemma. First, if one cannot trap a 'primary intermediate' at liquid helium temperatures, then it is not clear that we are dealing with a spectral event associated with an intermediate (which implies a potential energy minimum along the reaction surface) or a spectral event characteristic of a slow relaxation process. For the purposes of this discussion, therefore, we will treat bathorhodopsin as the primary photoproduct, but note that one or more ground-state relaxation processes, involving the chromophore as well as nearby protein residues, are involved in its formation.

IV-A. Models of the primary event

Our model of the primary event in vertebrate rhodopsin is shown in Fig. 10 [51]. This model is based on the 11-*cis* → 11-*trans* isomerization model originally proposed by Yoshizawa and Wald [330] and the binding site model shown in Fig. 5 and discussed in Section III. Although this model accommodates the major spectro-

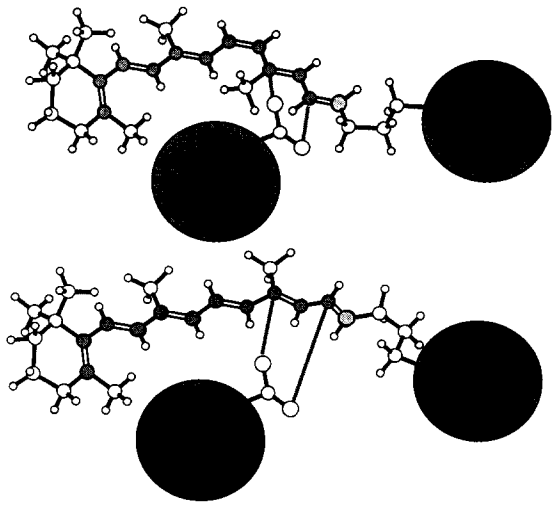

Fig. 10. A possible model of the primary photochemical event in rhodopsin based on the experimental and theoretical analyses of Ref. 51. Rhodopsin is shown in the top diagram and bathorhodopsin is shown in the bottom diagram. Key electrostatic interactions that stabilize the chromophore are shown by using dashed lines. The entire β-ionylidene ring, the α-carbon of the lysine residue and the counterion are assumed to be held stationary by the protein matrix during the phototransformations, so that all geometric relaxation is localized within the $C_7 \ldots N_{16} \ldots \beta\text{-}C_{lys}$ fragment. The counterion (an aspartic or glutamic acid residue) was approximated in the theoretical simulations by using a $CH_3\text{-}CO_2^-$ moiety [51]. The counterion (CTN) is not intimately associated with the imine proton in either rhodopsin or bathorhodopsin. The counterion lies underneath the plane of the chromophore in rhodopsin, and the primary chromophore-counterion electrostatic interactions involve C15-CTN and C13-CTN. Energy storage in bathorhodopsin (≈ 32 kcal·mol^{-1}) is approximately 60% conformational distortion and 40% charge separation.

scopic observations, there are a number of modifications that could be made which might also accommodate the available data. The purpose of this section is to evaluate the key elements of this model. This goal will be accomplished in part by comparing it to other models recently proposed in the literature.

The first issue that deserves examination is whether the primary event involves an isomerization. The observation that bathorhodopsin is generated in a few picoseconds prompted the suggestion that the primary event involved a proton translocation rather than an isomerization [251]. This suggestion was based in part on the assumption that an isomerization involving a large change in conformation would take 100–1000-times longer, but subsequent molecular dynamics calculations predicted picosecond isomerization times [54,55]. The controversy has been resolved by a series of spectroscopic studies which indicate that the chromophore in bathorhodopsin is an all-*trans* protonated Schiff base and that the primary photoproducts formed from isorhodopsin (9-*cis*) and rhodopsin (11-*cis*) are identical [24,48,72,73,82,92,110,129,156,169,212,213,219,229,246, 249,250,264,313,319]. Thus, the primary photochemical event in vertebrate rhodopsin involves an 11-*cis* to 11-*trans* photoisomerization. The recent observation of Foster and coworkers that *C. reinhardtii* can be activated even when 'non-isomerizable' chromophores are incorporated into the binding site [114,115,117] should not be used as ammunition against an isomerization during the primary event of vertebrate rhodopsin. It is clear from an analysis of the opsin shifts for various analogs (Fig. 8) that the binding site of *Chlamydomonas* rhodopsin is quite different from vertebrate rhodopsin. Furthermore, the possibility that *Chlamydomonas* can be activated via C=N photoisomerization remains an open question. Finally, the observations of Longstaff and Rando [127,203,205] indicate that deprotonation of the chromophore is required for activation of rhodopsin. Because deprotonation occurs upon the formation of metarhodopsin II, and metarhodopsin II is only formed after isomerization of the chromophore, it follows that isomerization of the chromophore is required for activation of native vertebrate rhodopsin. The latter observation, however, does not preclude the possibility that a chromophore analog might be found that deprotonates upon excitation, and that deprotonation of the chromophore may be sufficient to activate rhodopsin (see subsection IV-F). To date, no such analog for vertebrate rhodopsin has been found, however. In contrast, *C. reinhardtii* appears to be activated by virtually all chromophore analogs that form protonated Schiff bases within the binding site [114,115,117]. One possibility is that the chromophore in the binding site of *Chlamydomonas* rhodopsin is bound in a sufficiently unstable binding site that deprotonation (and perhaps expulsion) of the chromophore upon excitation can occur with, or without, concomitant isomerization. Regardless of the explanation, we conclude that the binding site and the activation mechanism of *C. reinhardtii* is distinctly different from that of vertebrate rhodopsin. Further work on *C. reinhardtii* is important, however, for it is often in understanding the differences between two nominally similar systems that new insights are gained.

The observation that the primary event of rhodopsin involves an 11-*cis* $\rightarrow$ 11-*trans* photoisomerization does not preclude concerted single or C=N double bond twists. The early 'Bicycle Pedal' model involving concerted torsion about two double bonds [323] and the more recent 'Hula Twist' model involving concerted torsion of the C11=C12 double bond and the adjacent C10–C11 single bond [198,202] are examples. Resonance Raman [221,249], FTIR [24,121,267,294] and analog studies [5,84,286,291], however, have provided strong evidence that only the C11=C12 bond isomerizes during the primary event. Thus, the primary event is a one-bond 11-*cis* to 11-*trans* photoisomerization of the chromophore. The complex motions of the lysine residue accompanying the chromophore isomerization remains

a subject of active experimental [223,277] and theoretical [41,51,324] study. We explore the key molecular and electronic features of the photochemical process below.

IV-B. Quantum efficiency of photoisomerization

The quantum yields for the photoconversions involving rhodopsin, bathorhodopsin and isorhodopsin are shown in Fig. 11 and the salient assignments are given below:

$$\text{rhodopsin (R)} \underset{\Phi_2 = 0.49}{\overset{\Phi_1 = 0.67}{\rightleftharpoons}} \text{bathorhodopsin (B)} \underset{\Phi_4(\lambda,T)}{\overset{\Phi_3 = 0.073}{\rightleftharpoons}} \text{isorhodopsin (I)}$$

where the values $\Phi_1 = 0.67 \pm 0.02$, $\Phi_2 = 0.49 \pm 0.03$, $\Phi_3 = 0.076 \pm 0.006$ are independent with respect to both temperature and excitation wavelength within the error ranges specified [48]. In sharp contrast, Φ_4 is observed to be both temperature- and wavelength-dependent [51,264,277]. This latter observation has interesting implications and will be the subject of the next section. The quantum yield of the primary event was originally assigned by Dartnall [79] and subsequent studies have yielded values in agreement within experimental error [48,169,264]. The observation that Φ_1 of rhodopsin is larger by a factor of at least two compared to the photoisomerization quantum efficiency of the 11-*cis*-retinyl protonated Schiff base (RPSB) in solution [118,119] is one indication that the protein has a binding site optimized for 11-*cis* → 11-*trans* photoisomerization. The fact that the primary event also stores about 32 kcal · mol^{-1} [66,75,277], whereas the photoisomerization of the 11-*cis*-RPSB in solution generates a more stable species, provides further evidence that the protein is modifying both the ground and the excited state potential surfaces. The observation that $\Phi_1 + \Phi_2$ add up to a number larger than unity (1.16 ± 0.05) indicates that, while a common excited state intermediate may be populated during photochemistry, coupling into the ground state is a trajectory dependent (i.e., dynamic) process (see below). A key conclusion is that the excited state C11=C12 torsional surface is barrier-less [39,41,48,51,55,92,152,156]. Interestingly, it appears that the C9=C10 torsional surface is not barrier-less (see below).

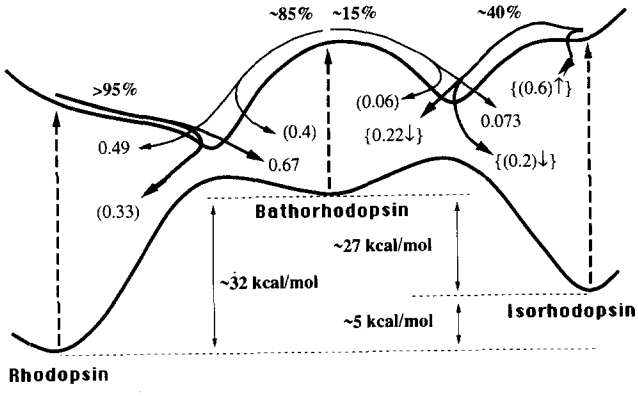

Fig. 11. Schematic representation of the ground and first excited singlet state surfaces connecting rhodopsin, bathorhodopsin and isorhodopsin using a simplified (linearized) reaction coordinate. The shapes of the ground and excited state surfaces are based on INDO-PSDCI calculations [51]. Ground-state enthalpies are taken from the experimental measurements of Cooper [74,75] and Schick et al. [277]. Absolute quantum yields of photoisomerization are displayed at the tips of the arrows indicating the processes [48,51]. Values given in parentheses (●) are predicted by using semiempirical molecular dynamics theory to calculate the reverse/forward yield ratios and multiplying these values by the experimental forward yields (shown without parentheses). Values listed in brackets {●} are ambient temperature quantum yields which display temperature dependence. The arrows indicate the effect that lowering the temperature will have on these values, e.g., {0.22↓} indicates that at lower temperatures, the quantum yield will be lower than 0.22. Reproduced with permission from Ref. 51.

IV-C. Origin of the isorhodopsin quantum yield wavelength dependence

At ambient temperature, the quantum efficiency of the isorhodopsin → bathorhodopsin phototransformation (Φ_4) equals 0.22 ± 0.03 and displays no wavelength dependence within the error range specified [169]. In contrast, at liquid nitrogen temperatures, isorhodopsin photochemistry displays a significant wavelength dependence. Measurements at seven wavelengths yielded values of Φ_4 ranging from a low of 0.089 ± 0.021 at 565 nm to a high of 0.168 ± 0.012 at 440 nm [51]. An analysis of these data based on a variety of kinetic models suggests that the I → B photochemistry is characterized by a small activation barrier (≈ 0.2 kcal · mol^{-1}) associated with the 9-*cis* ↔ 9-*trans* excited state torsional potential surface [51]. This barrier is sufficiently small that at ambient temperautre ($kT \cong 0.6$ kcal · mol^{-1}), thermal effects mask the presence of this barrier. In contrast, at 77 K ($kT \cong 0.15$ kcal · mol^{-1}), thermal energy and barrier height are comparable, and the wavelength dependence has its origin in the partitioning of excess vibrational energy into the C9=C10 torsional coordinate. A detailed spectroscopic and theoretical analysis of these data suggests that the origin of the excited state barrier in isorhodopsin arises primarily from electrostatic effects associated with the interaction of the counterion and the protonated species [51]. Low temperature picosecond studies of the primary event in isorhodopsin could provide new insights into the nature and characteristics of this barrier.

IV-D. Energy storage in the primary event

The first photocalorimetric measurement of the energy stored in the primary photochemical event of rhodopsin was carried out by Alan Cooper in 1979, and his measurement of $\Delta H_{RB} = 34.7 \pm 2.2$ kcal · mol^{-1} [75]

prompted considerable interest in the mechanistic origins. First, this value indicates that about 60% of the absorbed photon energy is converted into stored energy, an efficiency that seems unrealistically high given the concomitant high quantum efficiency of 0.67 (net system efficiency $\cong 40\%$). Second, models of the primary event published during the same year predicted much lower values: (e.g., 26 kcal · mol^{-1} [54] and 14–28 kcal · mol^{-1} [156]). A subsequent experimental study using a different technique (pulsed laser photocalorimetry) and a range of excitation wavelengths yielded $\Delta H_{RB} = 32.2 \pm 0.9$ kcal · mol^{-1} [277], in good agreement with Cooper's measurement. This study also measured the energy stored in the isorhodopsin → bathorhodopsin phototransformation and observed $\Delta H_{IB} = 27.1 \pm 3.2$ kcal · mol^{-1} [277]. This value of Δ_{IB} indicates that the bathorhodopsins formed from rhodopsin and from isorhodopsin are energetically equivalent, because isorhodopsin has an enthalpy about 5 kcal · mol^{-1} higher than rhodopsin [74]. This observation, combined with optical spectroscopic studies, confirms the fact that the bathorhodopsins formed from rhodopsin and isorhodopsin are identical [103,166,212,229]. A schematic showing the ground and excited state energetics is presented in Fig. 11.

There is no universally accepted model of energy storage, and some models emphasize energy storage due to charge separation [156] while others emphasize energy storage due to conformational distortion [54,55]. Virtually all models recognize that both mechanisms contribute, and discussions center on the extent to which one mechanism dominates the other. A recent experimental and theoretical study of energy storage in bathorhodopsin yielded the following partitioning: charge separation (≈ 12 kcal · mol^{-1}), intrachromophore-lysine conformational distortion (≈ 10 kcal · mol^{-1}), and chromophore-protein conformational distortion (≈ 10 kcal · mol^{-1}) [51]. The model predicts that a majority of the chromophore-protein conformational distortion energy involves the interaction of the $C_{13}(-CH_3)=C_{14}-C_{15}$=N-lysine moiety with nearby (unknown) protein residues [51].

IV-E. Molecular dynamics of the primary event

The primary event in rhodopsin is an 11-*cis* to 11-*trans* photoisomerization, a conformational change that involves rearrangement of a large fraction of the retinyl polyene (Fig. 10). The observation that bathorhodopsin forms in a few picoseconds [229,251] with a quantum yield of 0.67 [48,79,169,264] places rather severe constraints on the nature of the excited state dynamics. Birge and Hubbard carried out molecular dynamics calculations on the primary event and predicted a bathorhodopsin formation time of 2.3 ps with a quantum yield of 0.61 [41,54,55]. While these calculations were based on semiempirical molecular orbital and molecular dynamics procedures, and the model of the binding site had the counterion too close to the imine linkage, the qualitative features of the photoisomerization process are likely to be correct. We base this assumption in part on the fact that the theory predicted a bathorhodopsin → rhodopsin quantum yield of 0.48 [55], a value much larger than was currently accepted but which ultimately turned out to be reasonably accurate (see above).

The following observations of the primary event are possible:

(1) Excitation of rhodopsin into the lowest-lying Franck-Condon excited state generates a large redistribution of the charge resulting in the transfer of about 0.53 electron units of negative charge into the C11...N16 portion of the polyene chain. (Selected INDO-PSDCI charges (electron units $\times 10^3$) in the ground, vertical excited states are as follows: $C_{11}(68,-47)$, $C_{12}(-9,92)$, $C_{13}(103,-112)$, $C_{14}(-29,9)$, $C_{15}(244,13)$, $N_{16}(-86,-190)$, net charges C11...N16 (291, −235); data from Fig. 1 of Ref. 54.) This charge reorganization alters the electrostatic interaction with the counterion (e.g., Fig. 10) from a stabilization into a destabilization and forces the polyene away from the counterion. Torsion about the C11=C12 bond is the path of minimum energy, and thus the photoisomerization is initiated with a negative barrier.

(2) Torsion about the C11=C12 bond is calculated to mix the second excited '$^1A_g^{*-}$' state into the lowest-lying '$^1B_u^{*+}$' state. In the torsional region 75–105° (90° = orthogonal), the lowest excited state has considerable '$^1A_g^{*-}$' character (see Fig. 3, Ref. 54). This generates a local minimum in the excited state potential surface (see Fig. 11). This local minimum is reached in about 1 ps following excitation.

(3) The torsional trajectory is trapped in the local minimum and oscillates within this region with a frequency of about $4.5 \cdot 10^{12}$ Hz ($= 150$ cm^{-1}). Each pass of the molecule through the orthogonal dihedral region (where the ground and excited state surfaces come in closest proximity) transfers roughly one-third of the molecules into the ground state. The calculated quantum yield of 0.62 was obtained by following all of the trajectories, but an approximate analysis of quantum yield can be obtained by using the formula $\Phi \cong a/(1-(1-a)^2)$ where a is the average transfer probability [313]. An average of the probabilities of the first eight passes through the crossing region yields about 0.30 (Table I of Ref. 54) and the above formula predicts $\Phi = 0.59$. Weiss and Warshel have suggested that our formula for the crossing probability will underestimate the probability, and they propose that non-adiabatic coupling will increase a to about 0.5 [325]. This will yield a quantum yield of exactly 0.67, in much better agreement with experiment. However, their algorithm

apparently predicts the same quantum yield for the B → R photochemistry. Our procedures predict 0.48 [55], in much better agreement with the experimental value of 0.49 [48]. The lower quantum yield in going from bathorhodopsin to rhodopsin is due to the rapid arrival of the trajectory into the activated complex precluding equilibration of the excited state which enhances coupling (the surfaces are further apart energetically). Indeed, the average of the probabilities of the first eight passes through the crossing region yields $a = 0.031$ (Table II of Ref. 54) and the formula $\Phi \cong a/(1-(1-a)^2)$ predicts $\Phi = 0.51$. The molecular dynamics simulation predicts 0.48 because the forward crossing probability (R → B) is calculated to be slightly higher than the reverse crossing probability (B → R) due to the shape of the surface (see Ref. 54).

IV-F. Origin of photoreceptor noise in vivo

The weakest pulse of light that the human eye can reliably distinguish from background noise sends roughly 100 photons through the pupil and produces 10–20 activated rhodopsin molecules [4,30,36]. It has been proposed that single photon sensitivities are not possible due to dark noise associated with randomly occurring thermal isomerizations of the protein-bound chromophore in rhodopsin [4,30]. Indeed, Aho and co-workers have demonstrated that animals with low body temperature, which decreases the rate of thermal activation processes, have higher visual sensitivity [4]. They propose that thermal isomerizations are the key source of dark noise in both vertebrate and invertebrate visual systems [4]. In contrast, Barlow and co-workers have studied photoreceptor noise in *Limulus* and have concluded that thermal isomerization of the chromophore is unlikely to be the source of the dark noise [31,32]. The following section examines the viability of the thermal isomerization model.

Baylor and co-workers have carried out a detailed analysis of electrical dark noise in toad retinal rod outer segments, and assigned the thermodynamic properties of the thermally activated dark processes: ($E_a = 21.9 \pm 1.6$ kcal · mol^{-1}, $\Delta G^{\ddagger} = 31.9 \pm 0.13$ kcal · mol^{-1}, $\Delta H^{\ddagger} = 21.6 \pm 1.6$ kcal · mol^{-1}, $\Delta S^{\ddagger} = -35.3 \pm 5.6$ e.u.) [36]. The activation energies measured for *Limulus* are in agreement within experimental error ($E_a = 26.3 \pm 7.8$ kcal · mol^{-1} (day), 27.9 ± 6.5 kcal · mol^{-1} (night), 26.5 ± 7.5 kcal · mol^{-1} (in vitro)) [31,32]. A comparison of these data with denaturation activation energies measured by Hubbard for cattle rhodopsin ($E_a \approx 100$ kcal · mol^{-1}), frog rhodopsin ($E_a \approx 45$ kcal · mol^{-1}) and squid rhodopsin ($E_a \approx 72$ kcal · mol^{-1}) indicates that protein denaturation is not the origin of the dark signal [161]. Measurements of thermal isomerization of 11-*cis*-retinal, however, appear to offer a much more compatible set of thermodynamic properties ($E_a = 22.4$ kcal · mol^{-1}, $\Delta G^{\ddagger} = 29.3$ kcal · mol^{-1}, $\Delta H^{\ddagger} = 21.7$ kcal · mol^{-1}, $\Delta S^{\ddagger} = -21.4$ e.u.) (1-propanol solution) [162]. Comparison of the latter measurements on 11-*cis*-retinal with those observed by Baylor on rod segments has prompted some investigators to propose that thermal isomerization of the 'chromophore' is responsible for dark activation of rhodopsin [4,30,36]. Unfortunately, this hypothesis is not consistent with the energetics of ground state isomerization of the protein bound chromophore. As discussed in detail above, the protein bound chromophore is not 11-*cis*-retinal, but the protonated Schiff base of 11-*cis*-retinal. The ground state barrier to isomerization of the protein bound chromophore is estimated to be $\delta H^{\ddagger} = 45 \pm 3$ kcal · mol^{-1} (see Fig. 12). We can establish a lower limit of $\Delta H^{\ddagger} \geq 42 \pm 3$ kcal · mol^{-1} based on the relative enthalpy of bathorhodopsin ($\Delta H_{RB} = 32.2 \pm 0.9$ kcal · mol^{-1}) [277] plus the activation enthalpy of the bathorhodopsin → lumirhodopsin dark reaction ($\Delta H^{\ddagger} = 10 \pm 2$ kcal · mol^{-1}) [130] and assuming additive errors. Thus, thermal (ground state) isomerization of the native (protonated) chromophore cannot be responsible for thermal activation of the protein.

There are at least three alternative possibilities that are more likely than the thermal isomerization proposal. The first possibility is that rhodopsin can undergo a conformational change ($R \overset{\Delta}{\rightarrow} R^{**}$) that is interpreted (incorrectly) by transducin ($T_{\alpha\beta\gamma}$-GDP) to represent photochemically activated rhodopsin (R*). Thus the initial step in the amplification process takes place involving this thermally activated rhodopsin ($T_{\alpha\beta\gamma}$-GDP + R** → R**-$T_{\alpha\beta\gamma}$-GDP + GTP → R**-$T_{\alpha\beta\gamma}$-GTP +

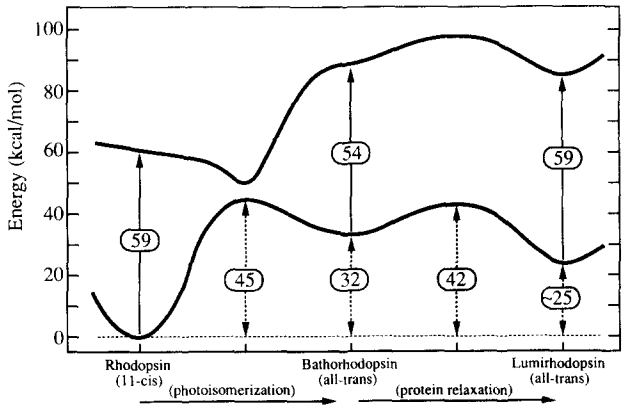

Fig. 12. The key energetic components of the ground and lowest excited singlet state potential surfaces asociated with the rhodopsin → bathorhodopsin → lumirhodopsin transformations. All energies are in kcal mol^{-1}. Solid arrows define Franck-Condon transition energies and dashed arrows define energies for maxima and minima in the potential surface relative to ground state rhodopsin. The energy of the primary photoproduct, bathorhodopsin, is based on pulsed laser photocalorimetric measurements (32.3 ± 0.9 kcal mol^{-1} [277]). The rhodopsin → bathorhodopsin ground state barrier is based on the analyses of Cooper et al. [74,75,76] and Honig et al. [156]. The activation enthalpy of the bathorhodopsin → lumirhodopsin dark reaction ($\Delta H^{\ddagger} = 10 \pm 2$ kcal · mol^{-1}) is from Grellman et al. [130].

GDP) (see Section II). The second possibility is that there is an equilibrium within the rhodopsin binding site coupling protonated versus unprotonated chromophores. Although spectroscopic studies indicate that less than 3% of rhodopsin molecules contain unprotonated Schiff base chromophores, this small population contains chromophores which will isomerize thermally with an activation energy very similar to that observed for retinal ($\Delta H^{\ddagger} \cong 22$ kcal $\cdot$ mol^{-1}) [162]. Finally, the experiments of Longstaff and Rando have demonstrated that deprotonation of the Schiff base of retinal is *obligate* for rhodopsin activation [203]. It is possible that deprotonation of the Schiff base is *sufficient* for activation. If so, the event that may be responsible for dark noise is thermally activated deprotonation of the chromophore. The activation energy of deprotonation and the lifetime of the deprotonated moiety are unknown, however, making this mechanism the most speculative of the three possibilities.

The above three hypotheses provide interesting alternatives to the current theory. All must be examined in greater detail before any should be taken seriously. An important observation that must be accommodated by any proposed mechanism is that the physiological signals that are generated via photon activation and thermal activation are identical in shape and amplitude [4,30,31,32,36]. The key point of the above discussion, however, is that thermal isomerization of the native (protonated) chromophore cannot be responsible because the enthalpy of isomerization ($\Delta H^{\ddagger} \cong 45 \pm 3$ kcal $\cdot$ mol^{-1}) is significantly larger than the enthalpy of the dark noise phenomenon ($\Delta H^{\ddagger} = 21.6 \pm 1.6$ kcal $\cdot$ mol^{-1}).

V. The primary photochemical event in light-adapted bacteriorhodopsin

Differential absorption changes associated with the first ~ 1 ps following excitation of light adapted bacteriorhodopsin are shown in Fig. 7 [220]. These data, and other spectroscopic measurements in the picosecond regime, are interpreted by most investigators to indicate the following sequence of events [220,238,253, 255]:

$$\text{bR(all-}trans\text{)} \xrightarrow{h\nu} \text{bR(FC)}^* \xrightarrow{\approx 100\,\text{fs}} \text{bR}(\tau_{13})^* \xrightarrow{\approx 300\,\text{fs}} \text{J (13-}cis\text{)}$$

$$\xrightarrow{\approx 5\,\text{ps}} \text{K (13-}cis\text{)}$$

where bR(FC)* represents the Franck-Condon (vertical) excited state, bR(τ_{13})* represents the excited state with the chromophore distorted out of the Franck-Condon region along the C13=C14 torsional coordinate, J is a 13-*cis* ground-state species and K is the first 'trappable' ground-state species. We define K as the primary photoproduct for reasons analogous to those discussed in the case of bathorhodopsin and the precursor photorhodopsin (Section IV). In other words, the fact that J cannot be trapped at lower temperatures may indicate that this species does not occupy a true ground state minimum, but simply represents an unrelaxed K species. Alternatively, Birge and co-workers have suggested the possibility that the absorption band attributed to J is associated with a mixture of ground-state and excited-state species [53]. Mathies and co-workers disagree and suggest that the time-resolved data shown in Fig. 7 are more consistent with a fully populated ground state within the formation time of J [220]. The latter assignment might appear more consistent with an analogy with rhodopsin photochemistry (photorhodopsin ≡ J; bathorhodopsin ≡ K). However, based on the kinetics, a more consistent analogy is (photorhodopsin ≡ K; bathorhodopsin ≡ KL). For the purposes of this discussion we will assume J is an unrelaxed ground-state precursor to K with both species having a 13-*cis* chromophore geometry.

V-A. Models of the primary event

Our model of the primary photochemical event in light-adapted bacteriorhodopsin is shown in Fig. 13. This model is based on the binding site geometry assigned in Section III and shown in Fig. 5b. Molecular orbital and molecular dynamics calculations based on this model reproduce the energetics ($\Delta H_{calc} = 14.9$ kcal $\cdot$ mol^{-1}; $\Delta H_{obs} = 16 \pm 3$ kcal $\cdot$ mol^{-1}), dynamics ($\tau_{calc} = 656$ fs, $\tau_{obs} \cong 500$ fs) and quantum yield ($\Phi_1 = 0.259$ (0.33 observed), $\Phi_2 = 0.738$ (0.67 observed) at 77 K) of the primary event observed at 77 K [50,52,53]. However, these observations should not be interpreted as support for the model shown in Fig. 5b versus Fig. 5c, because the geometry was manipulated to maximize agreement with experiment.

The conformational changes in the chromophore shown in Fig. 13 (bR (all-*trans*, 6-s-*trans*, C=N *anti*), J,K (13-*cis*, 6-s-*trans*, C=N *anti*)) are in general agreement with the models proposed by Mathies and co-workers based on resonance Raman studies [67,112, 219,221,299,300,302], Rothschild and co-workers based on FTIR studies [3,68,99,100,260,261,262,265,269,270, 271], and Griffin and co-workers based on NMR studies [136,137,298]. However, the assignment of the primary counterion to ASP-212 is based on the arguments presented in subsections III-A, B and D. The advantage of the model shown in Fig. 13 is that the imine proton, which is known to be involved in the proton pumping photocycle, is translocated in the direction of the pumping process upon primary photochemistry. This model is also in good agreement with the transient photovoltage measurements during the first 30 ps (see discussion in subsection III-D). Alternative models in which the chromophore is rotated by about 180 degrees (e.g., Fig. 5c), however, are more consistent with neutron diffraction data [145,146] and linear di-

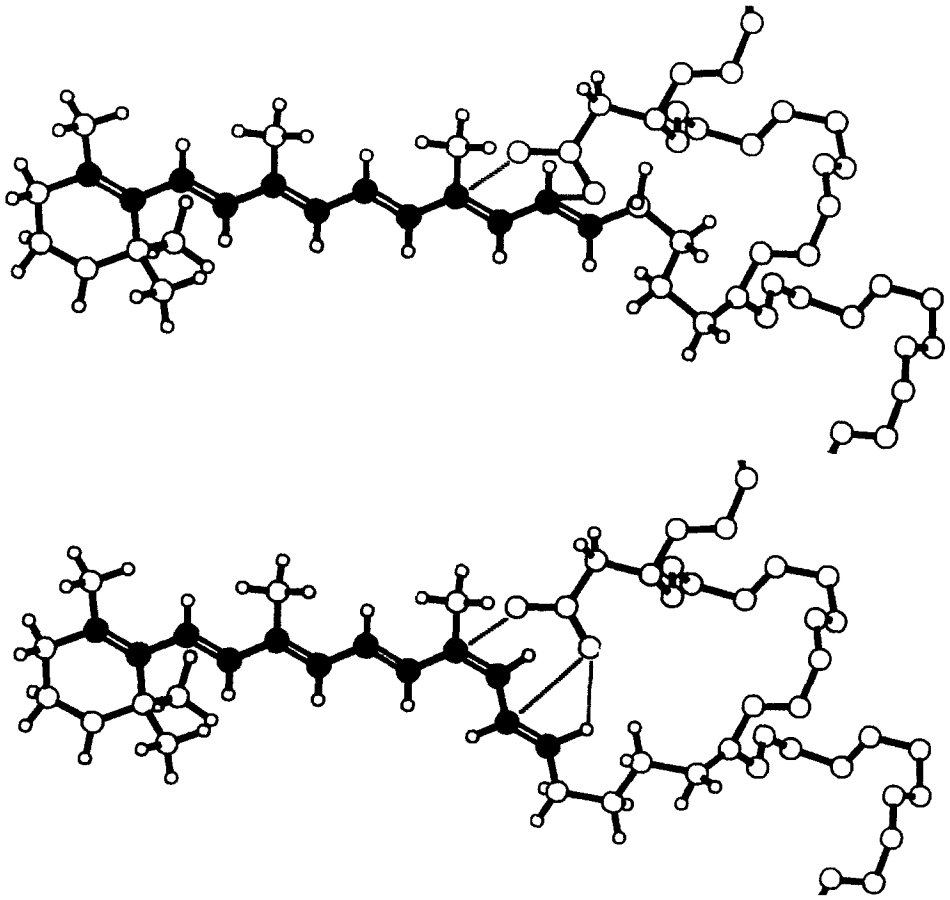

Fig. 13. A model of the primary photochemical event in light-adapted bacteriorhodopsin based on the binding site geometry shown in Fig. 5b. These two structures are labelled bR_1 (top) and K_1 (bottom), and yield the potential surfaces and excited state trajectories shown in the left rectangle in Fig. 14. An alternative pair of structures, labelled bR_2 and K_2 can be generated by moving the chromophore away from the counterion by a slight rotation of the entire polyene chromophore about the $\beta-\gamma$ lysine bond. This rotation decreases electrostatic stabilization of the all-*trans* chromophore in bR_2 and results in a smaller amount of energy storage in the primary photoproduct K_2 (right rectangle in Fig. 14). The location of the counterion, the entire β ionylidene ring and the lysine residue atoms fixed via attachment to the α-helix were (arbitrarily) held stationary during the isomerization. This was a required constraint because these degrees of freedom were manipulated to best reproduce the experimental spectroscopic and energetic properties.

chroism spectra [194]. We conclude that the orientation of the chromophore with respect to this counterion is an open issue.

There is one popular, alternative model which deserves mention. Tavana and Schulten have proposed that the primary photochemical event involves a concerted isomerization from 13-*trans*,14-s-*trans* to 13-*cis*,14-s-*cis* [280,281,314,315]:

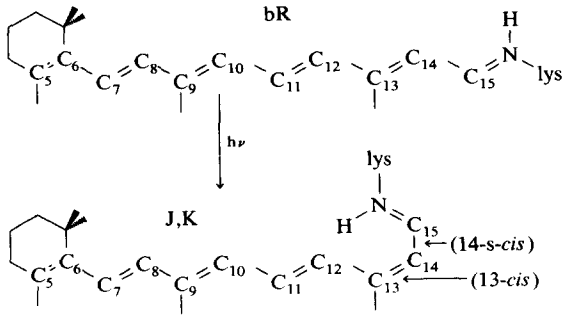

Although FTIR [122] and picosecond [253] experiments have been reported to be consistent with this model, there are three problems with the notion of a concerted 13,14-*cis* primary event that preclude enthusiasm. First, the kinetics of the primary event as well as the wavelength and temperature independence of the quantum efficiency of the primary event requires a barrier-less excited state surface coupling bR and the primary photoproduct (see below). It is unlikely that a concerted photochemical reaction involving the simultaneous rotation about two polyene bonds would produce a barrier-less excited state surface. Second, the detailed resonance Raman studies of Mathies and coworkers are not consistent with a 14-s-*cis* geometry in K or L [112,113,299,304]. (However, Tavan and Schulten have presented MNDO calculations which contradict the Raman assignments [315].) Third, photostationary state spectroscopic studies are inconsistent with a 13,14-*cis* primary photoproduct [50]. The mole fraction of K

(χ_K^{500}) in the 77 K, 500 nm photostationary state is observed to equal 0.46 ± 0.04 [50]. The calculated absorption spectrum of K at 77 K has a maximum absorbance at 620 nm, and a molar absorptivity at λ_{max} of 63900 $M^{-1} \cdot cm^{-1}$. The oscillator strength associated with excitation into the λ_{max} band, f_K, is determined to be 0.95 based on log-normal regression analysis [50]. The corresponding values for bR at 77 K are: $\lambda_{max} = 577$ nm, $\epsilon_{max} = 66100\ M^{-1} \cdot cm^{-1}$, and $f_{bR} = 0.87$. The observation that $f_K > f_{bR}$ is consistent with the displacement of the C15=NH portion of the retinyl chromophore away from a negatively charged counterion as a consequence of the all-*trans* to 13-*cis* photoisomerization. It is difficult to reconcile the observation that $f_K > f_{bR}$ with the proposal that the primary event involves an all-*trans* to 13-*cis*,15-s-*cis* photoisomerization, because the latter geometry is predicted to have a significantly lower λ_{max} band oscillator strength relative to the all-*trans* precursor, regardless of counterion location.

V-B. Molecular dynamics of the primary event

Molecular dynamics simulations based on the primary event model shown in Fig. 13 predict complex dynamics and biphasic repopulation of the ground state following excitation of bR (Fig. 14). The calculations shown in the left rectangle are reproduced from Ref. 53 are based on the model shown in Fig. 13. Roughly one-third of the excited molecules are trapped in an excited state potential well, and decay back to the ground state via non-dynamic processes. The simulations predict that this S_1^* potential well has a 13-transoid minimum so that decay of those species trapped in this well preferentially regenerate bR. The ground state conformation of bR (referred to as bR_1) assumed in the calculations shown on the left was optimized to reproduce as accurately as possible the optical and photocalorimetric data at 77 K. The calculations shown in the rectangle at right were carried out by allowing for a smaller amount of energy storage in the primary event and arbitrarily moving the entire chromophore away from the counterion by rotating about the β–γ lysine bond (top diagram of Fig. 13). This change decreases electrostatic stabilization of the all-trans chromophore, and shifts the S_1^* potential well to a 13-cisoid conformation. We refer to this geometry as bR_2. The molecular dynamics calculations predict that roughly one-third of the bR_2 molecules excited into the lowest singlet state are trapped in this S_1^* potential well and preferentially decay to form product (J or K). The calculations predict that a small change in ground state geometry produces a dramatic increase in the primary quantum yield [$\Phi_1(bR_1) = 0.266$; $\Phi_1(bR_2) = 0.743$] [50]. Because the probability of coupling into the ground state is relatively low for each trajectory (average crossing probability is less than 10% for the first ten passes over the orthogonal crossing region), the quantum yield sums are very close to unity for both geometries [$(\Phi_1 + \Phi_2)(bR_1) = 1.004$; $(\Phi_1 + \Phi_2)(bR_2) = 1.02$]. Although the bR_2 geometry is calculated to have a higher chromophore-counterion energy (≈ 2 kcal $\cdot$ mol^{-1}) relative to the bR_1 geometry (based on the binding site model of Ref. 25), the bR_2 geometry may be more stable when the entire protein energy is taken into account. Thus, there are two forms of light adapted bacteriorhodopsin which have very similar geometries, ground state energies and spectroscopic properties, but sigificantly different photochemical and energy storage characteristics.

V-C. The quantum efficiency of the primary event

Despite extensive experimental study [37,50,52,125, 168,171,239,240,253] assignment of the primary photochemical quantum yield of light-adapted bacteriorhodopsin remains a subject of controversy. As can be seen by reference to Table IV, measurements of Φ_1 range from a low of 0.25 [124] to a high of 0.79 [240]. This measurement range is in sharp contrast to the agreement that is observed in the literature with respect to the measurement of the primary quantum yield for vertebrate rhodopsin photochemistry (see Section IV-B). A closer examination of the data presented in Table IV indicates that all of the experimental measurements fall into one of two categories – those that predict $\Phi_1 = 0.33$ or below and those that predict $\Phi_1 = 0.6$ or above. No experimental measurements fall into the large intermediate range spanning from 0.34 to 0.59. If experimental uncertainty were the dominant source of the discrepancies in the measured quantum yields, one would predict that a majority of the measurements would fall into this intermediate range in contrast to none at all. Thus, the data in Table IV supports the concept that there are two types (or conformational states) of bacteriorhodopsin, one that has a forward quantum yield of approximately 0.3 and a second that has a forward quantum yield of 0.6. Before we accept this interpretation, however, it is important to consider alternative explanations that may be responsible for producing systematic errors capable of generating an apparent duality.

Kouyama et al. have examined the influence of the N intermediate on the bacteriorhodopsin photocyle [182]. The N intermediate has a major absorption maximum very close to that of bacteriorhodopsin and is photoactive. Kouyama et al. propose that at high pH and high light intensity, the overall photoreaction of bacteriorhodopsin may be approximated by the two-photon cycle,

$$bR \xrightarrow{h\nu} K \rightarrow L \rightarrow M \rightarrow N \xrightarrow{h\nu} ({}^{N}L \Leftrightarrow {}^{N}M) \rightarrow bR,$$

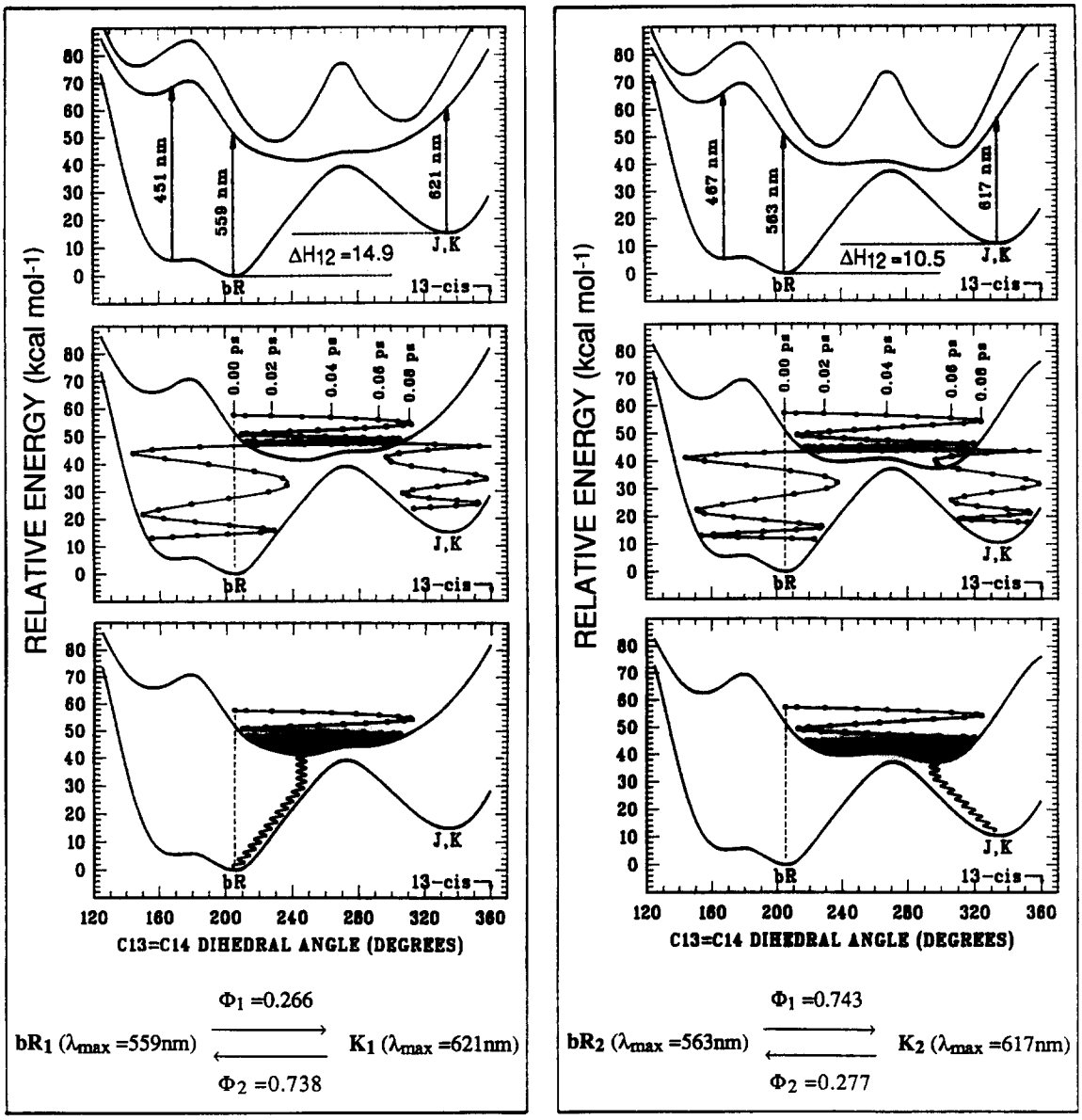

Fig. 14. Potential energy surfaces and molecular dynamics of the primary photochemical transformation of light adapted bacteriorhodopsin based on two different models of the binding site (Fig. 13). The ground and excited state surfaces are defined in reference to the principal torsional coordiante [τ(C12–C13=C14–C15)] and were generated by adiabatic minimization of all labile lysine internal coordinates as well as the following polyene stretching (R), bending (<), and torsional (τ) coordinates: R(C11=C12), R(c12–C13), R(C13=C14), R(C14–C15), R(C15=N16), < (C11=C12–C13), < (C12–C13=C14), < (C13=C14–C15), < (C14–C15=N16), τ(C10–C11=C12–C13), τ(C11=C12–C13=C14), τ(C12–C13=C14–C15), and τ(C13=C14–C15=N16). The calculations shown in the left rectangle ($bR_1 \rightarrow K_1$) are from Ref. 53 and are based on the binding site model shown in Fig. 13. The calculations shown in the rectangle at right ($bR_2 \rightarrow K_2$) were carried out by allowing for a smaller amount of energy storage in the primary event by arbitrarily displacing the entire chromophore away from the counterion by rotating about the $\beta-\gamma$ lysine bond [50]. All dynamics were carried out by using Lagrangian interpolation on the ground and excited state surfaces to define the steepest decent gradients (see Appendix of Ref. 55). The equations of motion were solved and the positions of the nuclei updated in temporal increments of 0.1 fs. The probability of crossing from the excited state into the ground states was calculated by using the semiclassical S matrix methods described by Birge and Hubbard [54,55]. While these methods are approximate, identical methods were used to simulate rhodopsin photochemistry, and the calculated quantum yields ($\Phi_1 = 0.62$, $\Phi_2 = 0.48$) are in reasonable agreement with the observed values ($\Phi_1 = 0.67$, $\Phi_2 = 0.49$) (see subsection IV-E).

whereas at neutral pH and low light intensity, it can be described by the one-photon cycle

$$bR \xrightarrow{h\nu} K \rightarrow L \rightarrow M \rightarrow N \rightarrow O \rightarrow bR.$$

Thus, the above two schemes could account for anomalies in quantum yield measurements at ambient temperatures involving the observation of M. For example, the presence of the two-photon cycle would artificially de-

crease the measured quantum yield of M formation by up to one-half. Thus, if we assume $\Phi_1 \approx 0.6$, a continuous wave experimental measurement at high pH and high light intensity could yield about 0.3, because roughly one-half of the photons absorbed would be absorbed by N, which has an absorption spectrum very similar to bR. While it is possible that some of the measurements reported in Table IV might have been affected by this competitive absorption phenomenon, a majority were not. Thus, we must seek alternative explanations.

A cursory examination of Table IV suggests that temperature might be responsible for generating a decreased forward quantum yield. This is an important possibility to investigate, because a small barrier in the excited state potential surface, rather than two forms of bacteriorhodopsin, could be the source of the observed duality. Indeed, isorhodopsin photochemistry displays a temperature dependent quantum yield due to a very small barrier in the excited state (see subsection IV-C). While it is true that all of the measurements resulting in the values of $\Phi_1 \geq 0.6$ were carried out at ambient temperature, two ambient temperature measurements yielded values in the range 0.25–0.31. Thus, temperature is not uniquely responsible for generating the large differences in Φ_1.

Two of the three ambient temperature measurements generating values of $\Phi_1 > 0.6$ were carried out by measuring the formation of M in high salt, ether solution. Diethyl ether is known to increase the lifetime of the M intermediate [37,240], although the mechanism is not understood. It is also known that salt concentration has a dramatic effect on the quantum yield of proton translocation [65,128,215,216,217]. Recent investigations suggest that the nature of the photocycle is dramatically affected by pH [78,134]. These latter studies suggest that there are at least two independent photocycles for light adapted bacteriorhodopsin, one which is responsible for generating M_{fast}, and a second which is responsible for generating M_{slow}. A third photocycle may be responsible for generating the recently observed intermediate called R [78,95,126]. Thus, a distribution of photocycles may exist. There is additional information that supports the concept of at least two photocycles. A number of investigators have proposed the presence of branching points and/or parallel pathways in the photocycle [26,27,104,176,181,195]. Hanamoto et al. proposed that there are two forms of M that are alternately populated depending upon the ionization state of an apoprotein moiety with a pK near 9.6 [134]. Iwasa et al. [172] and Balashov et al. [26,27] have proposed the existence of two forms of bR and K. Similarly, Alshuth et al. have proposed the existence of two forms of L [10]. There is strong evidence to indicate that there are

TABLE IV

Literature assignments of the primary quantum yields of light-adapted bacteriorhodopsin

Investigators [a]	Φ_1 [b]	Φ_2 [c]	Φ_1/Φ_2	$\Phi_1 + \Phi_2$	T [d]	Reaction [d]	Conditions [e]
O&H (1973)	**0.79** [f]	–	(> 0.78)	–	300	bR → M	HS/ether
GOD (1976)	–	–	**0.40**	–	300	bR ⇔ K	aqueous
B&E (1977)	**0.30 ± 0.03**	**0.77 ± 0.12**	0.39 ± 0.15	1.07 ± 0.15	233	bR ⇔ M	glycerol
GKRO (1977)	**0.25 ± 0.05**	**0.63 ± 0.20**	0.40 ± 0.18	0.88 ± 0.25	300	bR ⇔ K	aqueous
H&E (1978)	**0.33 ± 0.05**	**0.67 ± 0.04**	0.49 ± 0.10	1.00 ± 0.09	77	bR ⇔ K	glycerol
OHT (1985)	**> 0.6**	–	(> 0.6)	–	300	bR → M	HS/ether
P et al. (1986)	**~ 0.6**	–	(≥ 0.6)	–	300	bR → K	aqueous
B et al. (1989)	< 0.49	–	**0.45 ± 0.03**	< 1.49	77	bR ⇔ K	glycerol

[a] Investigators are defined as follows:
GOK (1976) Goldschmidt et al. [125]; O&H (1973) Oesterhelt and Hess [240];
GKRO (1977) Goldschmidt et al. [124]; B&E (1977) Becher and Ebrey [37];
OHT (1985) Oesterhelt et al. [239]; H&E (1978) Hurley and Ebrey [168];
B et al. (1989) Birge et al. [50]. P et al. (1986) Polland et al. [253];

[b] Quantum yield for the formation of the primary photoproduct, K, from bR. Boldface numbers indicate direct measurements. Some investigators assigned this value by measuring the quantum yield of the bR → M photoreaction and by assuming that the quantum yield for the bR → M photoreaction isidentical tothat for the bR → K reaction (i.e., no branching back to bR occurs during the dark steps).

[c] Quantum yield for the formation of bR from the primary photoproduct, K. Boldface numbers indicate direct measurements. Some investigators assigned this value by measuring the quantum yield of the M → bR photoreaction and by assuming that the quantum yield for the M → bR photoreaction is identical to that for the K → bR reaction.

[d] The measurement temperature (in Kelvin) and the photoreaction studied. The symbol '⇔' is used to represent a photostationary state measurement.

[e] Solvent conditions used in the experimental measurement. When specific solvent conditions are not provided, 'aqueous' is assumed. HS represents high salt, and 'glycerol' conditions are typically mixtures of glycerol and water. Individual references should be consulted for more detailed descriptions of the experimental conditions.

[f] Values shown in boldface were measured directly and the error ranges, when reported, are those provided by the investigators. Remaining values in the same row were derived from the data in boldface.

different conformational states of bacteriorhodopsin [86,149]. All of these observations are consistent with the concept of two (or more) photocycles.

A key observation that can be made by reference to Table IV is that all photostationary state measurements yield values of Φ_1 near 0.3 and all direct measurements yield values of Φ_1 near 0.6. It is therefore tempting to propose that there is some systematic error that is affecting one type of measurement, but not the other. While this explanation cannot be ruled out, it is very unlikely. Photostationary state measurements on rhodopsin yield results identical to those obtained via direct measurements [48]. Furthermore, many of the investigators carrying out the photostationary state measurements listed in Table IV carried out similar 'successful' measurements on rhodopsin, which argues against experimental incompetence. Finally, a careful reading of those papers that predict Φ_1 near 0.6 indicates that the investigators took care to avoid systematic errors of the type that might overestimate the primary quantum yield. We conclude that systematic errors are unlikely to be responsible for the observed duality in the experimental measurements of the primary quantum yield.

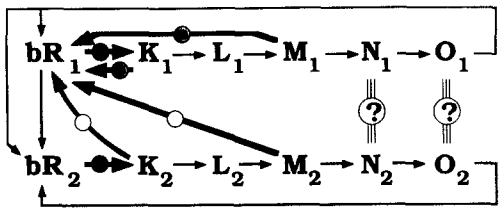

Fig. 15. A dual photocycle model of bacteriorhodopsin which rationalizes the experimental observation that all direct measurements on Φ_1 yield values greater than or equal to 0.6, while *all* photostationary state measurements on Φ_1 yield values less than or equal to 0.33. The thick arrows indicate photochemical transformations, and the quantum efficiency of the photochemical transformations are indicated by using filled circles: white (Φ unknown), black ($\Phi \approx 0.3$), grey ($\Phi \approx 0.6$). The thin arrows indicate thermal transformations. Thus, the bR_2 photocycle, which has the higher primary quantum yield, is the thermally more stable. Direct measurements will yield high values for Φ_1, because the $bR_2 \xrightarrow{h\nu} K_2$ photoreaction will be selected. However, the back reaction is not $K_2 \xrightarrow{h\nu} bR_2$ but rather $K_2 \xrightarrow{h\nu} bR_1$. Subsequent photochemistry will take place within the bR_1 photocycle, which will select the $bR_1 \xrightarrow{h\nu} K_1$ photoreaction, and yield a lower primary quantum yield. Because the reverse photoreaction from K_1 also selects bR_1, all photostationary measurements will measure the $bR_1 \xrightarrow{h\nu} K_1$ quantum yield, which is about 0.3. At some stage in the photocycles, the intermediates of the two photocycles may be equivalent (i.e., $N_1 \equiv N_2$, and $O_1 \equiv O_2$). Thus, bR_2 could be formed via thermal relaxation of bR_1 or directly via $O_1 \equiv O_2$.

Photophysical origins of the quantum yield duality

The discussion above provides evidence that there are two forms of bacteriorhodopsin, each with a characteristic photocycle. We will adopt the labels bR_1 and bR_2 to indicate these two forms, following the theoretical model presented in Fgis. 13 and 14. In this section we will explore the possible external stimuli that may be responsible for preferentially selecting one form over the other.

Analysis of the data of Table IV suggests that whatever perturbation is responsible for preferentially selecting bR_1 versus bR_2, it is difficult, if not impossible, to populate both forms simultaneously. Otherwise, we would observe quantum yield values characteristic of averages of bR_1 and bR_2. As discussed in the previous section, solvent, temperature, ionic strength and pH may affect the distribution of these photocycles in a complex way that remains to be explored in detail. However, it is difficult to rationalize why any of these environmental perturbations would force population of one form of bR versus another and avoid the generation of a thermodynamic equilibrium containing both.

Birge and coworkers have proposed that photochemistry, rather than environment, is the key selector of photocycle [50,52]. This proposal is based on the observation that all direct experimental measruements on Φ_1 yield values greater than or equal to 0.6, while all photostationary state measurement on Φ_1 yield values less than or equal to 0.33. This observation suggests a dual photocycle system as depicted in Fig. 15. The thick arrows in this figure indicate photochemical transformations while the thin arrows indicate thermal transformations. Thus, the bR_2 photocycle, which has the higher primary quantum yield, is the thermally more stable. Direct measurements will yield high values for Φ_1, because the $bR_2 \xrightarrow{h\nu} K_2$ photoreaction will be selected. However, the back reaction is not $K_2 \xrightarrow{h\nu} bR_2$ but rather $K_2 \xrightarrow{h\nu} bR_1$. Subsequent photochemistry will take place within the bR_1 photocycle, which will select the $bR_1 \xrightarrow{h\nu} K_1$ reaction, and yield a lower primary quantum yield. Because the reverse photoreaction from K_1 also selects bR_1, all photostationary measurements will measure the $bR_1 \xrightarrow{h\nu} K_1$ quantum yield, which is about 0.3.

It is possible that a change in the ionization state of a group on the apoprotein, rather than a change in the chromophore-counterion geometry (Fig. 13), is responsible for transforming bR_1 to bR_2. The recent studies of El-Sayed and co-workers [134] provide support for this alternative hypothesis. These investigators proposed that the biphasic kinetics observed in the formation of M are associated with two different chromophore environments provided by the apoprotein [134]. They proposed further that the two forms are alternately populated depending upon the ionization state of an apoprotein moiety with a pK near 9.6. Regardless of which of the above alternatives is assigned as the dominant mecha-

nism for selecting bR_1 versus bR_2, the key proposal is that a small change in protein geometry or binding site electrostatic environment can have a dramatic effect on the primary quantum yield.

V-D. Energy storage in the primary event

Birge and Cooper measured the energy stored in the primary photochemical event of light adapted bacteriorhodopsin to equal 15.8 ± 2.5 kcal $\cdot$ mol^{-1} based on pulsed laser photocalorimetry at 77 K [49]. This assignment assumed the bR $\Leftrightarrow$ K quantum yields measured by Hurley and Ebrey (see Table IV) [168]. The controversy concerning the assignment of the primary quantum yield, however, prompted a reevaluation of this assignment. A recent study indicates that the above energy storage value is valid for 77 K, but may be an overestimate of energy stored under experimental conditions that yield higher quantum yields [50]. Under the experimental conditions used in the photocalorimetry experiment [49], the energy stored in the K intermediate can be assigned by using the following equation [50],

$$\Delta H_K \text{ (kcal} \cdot \text{mol}^{-1}) \cong \frac{1}{3}\left\{\frac{4.71}{\Phi_1} + \frac{12.0}{\Phi_2} + \frac{1}{(0.10\Phi_2 + 0.0079\Phi_1)}\right\}$$

where Φ_1 is the forward quantum yield and Φ_2 is the reverse quantum yield for the interconversion bR $\Leftrightarrow$ K. Although the photocalorimetry and stationary state spectroscopic experiments cannot determine Φ_1 or Φ_2 directly, it is possible to assign the ratio Φ_1/Φ_2 independently. The observed number ($\Phi_1/\Phi_2 = 0.45 \pm 0.03$ [50]) is in good agreement with the Hurley and Ebrey measurement ($\Phi_1/\Phi_2 = 0.49 \pm 0.10$ [168]), and not compatible with the measurements yielding values of $\Phi_1 > 0.5$. Thus the photocalorimetric energy assignment is internally consistent, but is not necessarily applicable to environments that select quantum yields of 0.6 or above. We anticipate that energy storage for bR in environments that select quantum yields of 0.6 or above is smaller, and can be estimated to be about 10 kcal $\cdot$ mol^{-1} [50]. The implications of this prediction are discussed below.

V-E. Energy storage and proton pumping capability

Steady state illumination of intact cells induces the light adapted form of bacteriorhodopsin to eject one or more protons from the cytoplasm generating an electrochemical gradient across the cell membrane. This gradient can be partitioned into two components [52,56,185, 187,225,226],

$$\Delta p = \Delta\psi - 2.3RT\Delta\text{pH}/F \quad (2)$$

$$= \Delta\psi - 59\Delta\text{pH (mV at 25 °C)} \quad (3)$$

where Δp is the protonmotive force (or electrochemical gradient), $\Delta\psi$ is the electrical potential difference across the membrane and ΔpH is the pH gradient across the membrane. Eqn. 2 is obtained by evaluating RT/F (R = gas constant, F = Faraday constant) at $T = 298$ K. The pH gradient during illumination is dependent upon extracellular pH as well as other factors and is thus subject to uncertainty. Estimates of ΔpH generally range from 0.7 to 1.5 units (inside alkaline) [185,225,226]. Estimates of $\Delta\psi$ during illumination generally span the range from -120 to -220 mV [185,225,226]. Thus, the electrochemical gradient across the cell may reach about 350 mV, but for the purposes of this discussion we will assume an average gradient of 250 mV ($= -\Delta p$).

The free energy required to pump a single proton across a gradient of 250 mV is about 6 kcal $\cdot$ mol^{-1} (1 kcal $\cdot$ mol^{-1} = 43.4 mV/molecule). If we neglect entropy and assume the equivalence of enthalpy and free energy in estimating the relationship between energy storage and proton pumping capability, the energy stored in the primary event (about 16 kcal $\cdot$ mol^{-1}) is sufficient to pump two, but not three, protons per photocycle under typical ambient conditions. This maximum stoichiometry is consistent with many of the measurements of proton pumping stoichiometry, which indicate that two protons are pumped per photocycle [65,128,215–217]. However, those measurements yielding 2 protons/photocycle are typically based on an assumption that the primary quantum yield is about 0.3. In general, the actual observations yield

$$\text{protons pumped/photocycle} \cong 0.6/\Phi_1$$

and thus the proton pumping quantum yield will be closer to unity if Φ_1 is above 0.6. As noted above, however, environments that select photocycles with primary quantum yields of about 0.6 may result in a concomitant reduction in energy storage to about 10 kcal $\cdot$ mol^{-1} (e.g., Fig. 14). The latter energy storage value is consistent with a proton pumping stoichiometry no larger than one under ambient to high gradient conditions.

It is interesting to speculate on the potential biological relevance of our proposal that two photocycles may exist with different quantum yields and energy storage capacities. We will assign these two photocycles to have the following properties:

$$bR_1\{\Phi_1 \approx 0.3,\ \Delta H_{12} \approx 16 \text{ kcal} \cdot \text{mol}^{-1},$$

$$[H^+]/\text{photocycle} \approx 2(|\Delta p| \leq 250 \text{ mV}), \approx 1(|\Delta p| > 250 \text{ mV})\},$$

$$bR_2\{\Phi_1 \approx 0.6,\ \Delta H_{12} \approx 10 \text{ kcal} \cdot \text{mol}^{-1},$$

$$[H^+]/\text{photocycle} \approx 1(|\Delta p| \leq 250 \text{ mV}), \approx 0(|\Delta p| > 250 \text{ mV})\},$$

Following the model presented in Fig. 15, we assign bR_2 as the lower free energy form of the protein that is nominally active under in vivo conditions. Natural selection may have designed bacteriorhodopsin to inter-

convert from bR_2 to bR_1 under conditions of high electrochemical gradient ($|\Delta p| > 250$ mV) where bR_2 is no longer capable of pumping a proton because the free energy stored is insufficient to override the membrane gradient. Because bR_1 stores more energy in the primary event, it is a more efficient proton pump under conditions of high membrane electrochemical gradient. Analysis of the data of Table IV also suggests the possibility that bR_1 is photochemically selected via reverse photoreactions from K or M. Thus, under high light intensities, which will result in the generation of high electrochemical gradients, the protein is converted into the most efficient form. While the speculative nature of this discussion should be emphasized, we should not overlook the fact that the unusual photochemical properties of bacteriorhodopsin may have biological relevance.

Acknowledgements

The author thanks Drs. G.H. Atkinson, G.T. Babcock, S.P. Balashov, R.W. Barlow, R.A. Bogomolni, R.H. Callender, A. Cooper, T.G. Dewey, T.G. Ebrey, M.A. El-Sayed, K.W. Foster, J. Herzfeld, B. Honig, H.G. Khorana, D.S. Kliger, R.S.H. Liu, T. Marinetti, R.A. Mathies, D. Oesterhelt, M. Ottolenghi, R.R. Rando, K.J. Rothschild, T.P. Sakmar, M. Sheves, Y. Shichida, W. Stoeckenius and T. Yoshizawa for interesting and helpful discussions and for providing manuscripts prior to publication. Acknowledgement should not be interpreted as blanket endorsement by the above scientists of the analyses presented in this review. Research in the author's laboratory was funded in part by grants from the National Institutes of Health (EY-02202, GM-34548), the National Science Foundation (CHE-8516155; STC-8810879) and the Office of Naval Research (N00014-88-K-0359).

References

1 Adamus, G., McDowell, J.H., Arendt, A., Hargrave, P.A., Smyk-Randall, E. and Sheehan, J. (1987) in Biophysical Studies of Retinal Proteins (Ebrey, T.G., Frauenfelder, B., Honig, K. and Nakanishi, K., eds.), pp. 86–94, University of Illinois Press, Urbana.
2 Agard, D.A. and Stroud, R.M. (1982) Biophys. J. 37, 589–602.
3 Ahl, P.L., Stern, L.J., Hackett, N.R., Rothschild, K.J. and Khorana, H.G. (1987) Biophys. J. 51, 416 (abstr.).
4 Aho, A.C., Donner, K., Hyden, C., Larsen, L.O. and Reuter, T. (1988) Nature 334, 348–350.
5 Akita, H., Tanis, S.P., Adams, M., Balogh-Nair, V. and Nakanishi, K. (1980) J. Am. Chem. Soc. 102, 6370–6372.
6 Albeck, A., Friedman, N., Ottolenghi, M., Sheves, M., Einterz, C.M., Hug, S.J., Lewis, J.W. and Kliger, D.S. (1989) Biophys. J. 55, 233–241.
7 Albeck, A., Friedman, N., Sheves, M. and Ottolenghi, M. (1986) J. Am. Chem. Soc. 108, 4614–4618.
8 Alfano, R.R., Yu, W., Govindjee, Becher, B. and Ebrey, T.G. (1976) Biophys. J. 16, 541–545.
9 Alshuth, T. and Stockburger, M. (1981) Ber. Bunsen-ges. Phys. Chem. 85, 484–489.
10 Alshuth, T. and Stockburger, M. (1986) Photochem. Photobiol. 43, 55–66.
11 Applebury, M.L. and Volpp, K.J. (1987) in Biophysical Studies of Retinal Proteins (Ebrey, T.G., Frauenfelder, H., Honig, B. and Nakanishi, K., eds.), pp. 16–23, University of Illinois Press, Urbana.
12 Arnaboldi, M., Motto, M.G., Tsujimoto, K., Balogh-Nair, V. and Nakanishi, K. (1979) J. Am. Chem. Soc. 101, 7082–7084.
13 Asato, A.E., Denny, M., Matsumoto, H., Mirzadegan, T., Ripka, W.C., Gresatelli, F. and Liu, R.S.H. (1986) Biochemistry 25, 7021–7026.
14 Atkinson, G.H., Blanchard, D., Lemaire, H., Brach, T.L. and Harashi, H. (1989) Biophys. J. 55, 263–274.
15 Atkinson, G.H., Brach, T.L., Blanchard, D. and Rumbles, G. (1989) Chem. Phys. 131, 1–15.
16 Atkinson, G.H., Brack, T.L., Grieger, I., Rumbles, G., Blanchard, D. and Siemenkowski, L. (1986) Proc. SPIE-Int. Soc. Opt. Eng. 620, 82–88.
17 Aton, B., Doukas, A.G., Callender, R.H., Becher, B. and Ebry, T.G. (1977) Biochemistry 16, 2995–2999.
18 Aton, B., Doukas, A.G., Callender, R.H., Becher, B. and Ebry, T.G. (1979) Biochim. Biophys. Acta 576, 424–428.
19 Baasov, T., Friedman, N. and Shevers, M. (1987) in Biophysical Studies of retinal proteins (Ebrey, T.G., Frauenfelder, H., Honig, B. and Nakanishi, K., eds.), pp. 252–261, University of Illinois Press, Urana.
20 Baasov, T., Friedman, N. and Sheves, M. (1987) Biochemistry 26, 3210–3217.
21 Baasov, T. and Sheves, M. (1985) J. Am. Chem. Soc. 107, 7524–7533.
22 Baasov, T. and Sheves, M. (1985) Isr. J. Chem. 25, 53–55.
23 Baasov, T. and Sheves, M. (1987) J. Am. Chem. Soc. 109, 1594–1596.
24 Bagley, K., Balogh-Nair, V., Croteau, A.A., Dollinger, G., Ebrey, T.G., Eisenstein, L., Hong, M.K., Nakanishi, K. and Vittitow, J. (1985) Biochemistry 24, 6055–6071.
25 Bagley, K., Dollinger, G., Eisenstein, L., Singh, A.K. and Zimanyi, L. (1982) Proc. Natl. Acad. Sci. USA 79, 4972–4976.
26 Balashov, S.P. and Litvin, F.F. (1981) Biophys. 26, 566–581.
27 Balashov, S.P., Karneyeva, N.V., Imasheva, E.S. and Litvin, F.F. (1986) Biophysika 31, 1070–1073.
28 Baldwin, J.M., Henderson, R., Beckman, E. and Zemlin, F. (1988) J. Mol. Biol. 202, 585–591.
29 Balogh-Nair, V. (1987) in Biophysical Studies of Retinal Proteins (Ebrey, T.G., Frauenfelder, H., Honig, B. and Nakanishi, K., eds.), pp. 52–58, University of Illinois Press, Urbana.
30 Barlow, H.B. (1988) Nature 334, 296–350.
31 Barlow, Jr., R.B. and Kaplan, E. (1989) Biol. Bull. 177, 323.
32 Barlow, Jr., R.B. and Silbaugh, T.H. (1989) Invest. Ophthalmol. Vis. Sci. Suppl. 30, 61.
33 Barry, B., and Mathies, R.A. (1987) Biochemistry 26, 59–64.
34 Baselt, D.R., Fodor, S.P.A., Van der Steen, R., Lugtenburg, J., Bogomolni, R.A. and Mathies, R.A. (1989) Biophys. J. 55, 193–196.
35 Bayley, H., Huang, K.S., Radharkrishnan, R., Ross, A.H., Takagaki, Y. and Khorana, H.G. (1981) Proc. Natl. Acad. Sci. USA 78, 2225–2229.
36 Baylor, D.A., Matthews, G. and Yau, K.W. (1980) J. Physiol. 309, 591–621.
37 Becher, B. and Ebrey, T.C. (1977) Biophys. J. 17, 185–191.
38 Bennett, J.A. and Birge, R.R. (1980) J. Chem. Phys. 73, 4234–4246.
39 Birge, R.R. (1981) Annu. Rev. Biophys. Bioeng. 10, 315–354.
40 Birge, R.R. (1982) Methods in Enzymology 88, 522–533.
41 Birge, R.R. (1982) in Biological Events Probed by Ultrafast Laser

Spectroscopy (Alfano, R.R., ed.), pp. 299–317, Academic Press, New York.
42 Birge, R.R. (1983) in Ultrasensitive laser spectroscopy (Kliger, D.S., ed.), pp. 109–174, Academic Press, New York.
43 Birge, R.R. (1984) in Spectroscopy of Biological Molecules (Sandorfy, C. and Theophanides, T., eds.), pp. 457–471, D. Reidel, Boston.
44 Birge, R.R. (1986) Accts. Chem. Research 19, 138–146.
45 Birge, R.R., Bennett, J.A., Hubbard, L.M., Fang, A.L., Pierce, B.M., Kliger, D.S. and Leroi, G.E. (1982) J. Am. Chem. Soc. 104, 2519–2525.
46 Birge, R.R., Bennett, J.A., Pierce, B.M. and Thomas, T.M. (1978) J. Am. Chem. Soc. 100, 1533–1539.
47 Birge, R.R., Bocian, D.F. and Hubbard, L.M. (1982) J. Am. Chem. Soc. 104, 1196.
48 Birge, R.R. and Callender, R.H. (1987) in Biophysical Studies of Retinal Proteins (Ebrey, T., Frauenfelder, H., Honig, B. and Nakanishi, K., eds.), pp. 270–281, University of Illinois Press, Urbana.
49 Birge, R.R. and Cooper, T.M. (1983) Biophys. J. 42, 61–69.
50 Birge, R.R., Cooper, T.M., Lawrence, A.F., Masthay, M.B., Vasilakis, C., Zhang, C.F. and Zidovetzki, R. (1989) J. Am. Chem. Soc. 111, 4063–4074.
51 Birge, R.R., Einterz, C.M., Knapp, H.M. and Murray, L.P. (1988) Biophys. J. 53, 367–385.
52 Birge, R.R., Findsen, L.A., Lawrence, A.F., Masthay, M.B. and Zhang, C.F. (1989) in Biomolecular Spectroscopy (Birge, R.R. and Mantsch, H.H., eds.), pp. 103–112, The International Society for Optical Engineering, Bellingham, Washington.
53 Birge, R.R., Findsen, L.A. and Pierce, B.M. (1987) J. Am. Chem. Soc. 109, 5041–5043.
54 Birge, R.R. and Hubbard, L.M. (1980) J. Am. Chem. Soc. 102, 2195–2204.
55 Birge, R.R. and Hubbard, L.M. (1981) Biophys. J. 34, 517–534.
56 Birge, R.R., Lawrence, A.F., Cooper, T.M., Martin, C.T., Blair, D.F. and Chan, S.I. (1984) in Nonlinear Electrodynamics in Biological Systems (Adey, W.R. and Lawrence, A.F., eds.), pp. 107–120, Plenum, New York.
57 Birge, R.R., Murray, L.P., Pierce, B.M., Akita, H., Balogh-Nair, V., Findsen, L.A. and Nakanishi, K. (1985) Proc. Natl. Acad. Sci. USA 82, 4117–4121.
58 Birge, R.R., Murray, L.P., Zidovetzki, R. and Knapp, H.M. (1987) J. Am. Chem. Soc. 109, 2090–2101.
59 Birge, R.R. and Pierce, B.M. (1979) J. Chem. Phys. 70, 165–178.
60 Birge, R.R. and Pierce, B.M. (1983) in Photochemistry and Photobiology (Zewail, A.H., ed.), pp. 841–855, Harwood Academic, New York.
61 Birge, R.R., Pierce, B.M. and Murray, L.P. (1984) in Spectroscopy of Biological Molecules (Sandorfy, C. and Theophanides, T., eds.), pp. 473–485, D. Reidel, Boston.
62 Birge, R.R., Schulten, K. and Karplus, M. (1975) Chem. Phys. Lett. 31, 451–454.
63 Blanck, A. and Oesterhelt, D. (1987) EMBO J. 6, 265–273.
64 Blatz, P.E., Mohler, J.H. and Navangul, H.V. (1972) Biochemistry 11, 848–855.
65 Bogomolni, R.A., Baker, R.A., Lozier, R.H. and Stoeckenius, W. (1980) Biochemistry 19, 2152–2159.
66 Boucher, F. and Leblanc, R.M. (1985) Photochem. Photobiol. 41, 459–465.
67 Braiman, M. and Mathies, R. (1982) Proc. Natl. Acad. Sci. USA 79, 403–407.
68 Braiman, M.S., Mogi, T., Marti, T., Stern, L.J., Khorana, H.G. and Rothschild, K.J. (1988) Biochemistry 27, 8516–8520.
69 Braiman, M.S. and Rothschild, K.J. (1988) Annu. Rev. Biophys. Chem. 17, 541–570.
70 Braiman, M.S., Stern, L.J., Chao, B.H. and Khorana, H.G. (1987) J. Biol. Chem. 262, 9271–9276.
71 Buchert, J., Stefancic, V., Boukas, A.G., Alfano, R.R., Callender, R.H., Akita, H., Balogh-Nair, V., Nakanishi, K. and Pande, J. (1983) Biophys. J. 43, 279–283.
72 Callender, R.H., Doukas, A., Crouch, R. and Nakanishi, K. (1976) Biochemistry 15, 1621–1629.
73 Callender, R.H. and Honig, B. (1977) Annu. Rev. Biophys. Bioeng. 6, 33–55.
74 Cooper, A. (1979) FEBS Lett. 100, 382–384.
75 Cooper, A. (1979) Nature (Lond.) 282, 531–533.
76 Cooper, A. (1982) Methods Enzymol. 88, 667–673.
77 Crouch, R., Purvin, V., Nakanishi, K. and Ebrey, T. (1975) Proc. Natl. Acad. Sci. USA 72, 1538–1542.
78 Dancshazy, Z., Govindjee, R. and Ebrey, T.G. (1988) Proc. Natl. Acad. Sci. USA 85, 6358–6361.
79 Dartnall, H.J.A. (1972) in Handbook of Sensory Physiology (Heidelberg, ed.), pp. 122–145, Springer, Berlin.
80 De Groot, H.J.M., Harbison, G.S., Herzfeld, J. and Griffin, R.G. (1989) Biochemistry 28, 3346–3353.
81 DeGrip, W.J., Gray, D., Gillespie, J., Bovee, P.H.M., Van den Berg, H.M.M., Lugtenburg, J. and Rothschild, K.J. (1988) Photochem. Photobiol. 48, 497–504.
82 Deng, H. and Callender, R.H. (1987) Biochemistry 26, 7418–7426.
83 Deng, H., Pande, C., Callender, R.H. and Ebrey, T.G. (1985) Photochem. Photobiol. 41, 467–470.
84 Derguini, F. and Nakanishi, K. (1986) Photobiochem. Photobiophys. 13, 259–283.
85 Dewey, T.G. (1987) Biophys. J. 51, 809–815.
86 Diller, R. and Stockburger, M. (1988) Biochemistry 27, 7641–7651.
87 Dinur, U., Honig, B. and Ottolenghi, M. (1981) Photochem. Photobiol. 33, 523–527.
88 Dinur, U., Honig, B. and Schulten, K. (1980) Chem. Phys. Lett. 72, 493–497.
89 Dobler, J., Zinth, W. and Kaiser, W. (1988) Chem. Phys. Lett. 144, 215–220
90 Dollinger, G., Eisenstein, L. and Lin, S.-L. (1986) J. Am. Chem. Soc. 25, 6524–6533.
91 Dollinger, G., Eisenstein, L., Lin, S.L., Nakanishi, K. and Termini, J. (1987) in Biophysical Studies of Retinal Proteins (Ebrey, T.G., Frauenfelder, H., Honig, B. and Nakanishi, K., eds.), pp. 120–125, University of Illinois Press, Urbana.
92 Doukas, A.G., Junnarkar, M.R., Alfano, R.R., Callender, R.H. and Balogh-Nair, V. (1985) Biophys. J. 47, 795–798.
93 Doukas, A.G., Junnarkar, M.R., Alfano, R.R., Callender, R.H., Kokitani, T. and Honig, B. (1984) Proc. Natl. Acad. Sci. USA 81, 4790–4794.
94 Downer, N.W., Bruchman, T.J. and Hazzard, J.H. (1986) J. Biol. Chem. 261, 3640–3647.
95 Drachev, L.A., Kaulen, A.D., Skulachev, V.P. and Zorina, V.V. (1986) FEBS Lett. 209, 316–320.
96 Drikos, G., Morys, P. and Ruppel, H. (1984) Photochem. Photobiol. 40, 133–135.
97 Drikos, G., Rupel, H., Sperling, W. and Morys, P. (1984) Photochem. Photobiol. 40, 85–91.
98 Dunn, R., McCoy, J., Simsek, M., Majumdar, A., Chang, S.H., RajBhandary, U.L. and Khorana, H.G. (1981) Proc. Natl. Acad. Sci. USA 78, 6744–6748.
99 Earnest, T.N., Roepe, P., Braiman, M.S., Gillespie, J. and Rothschild, K.J. (1986) Biochemistry 25, 7793–7798.
100 Earnest, T.N., Roepe, P., Rothschild, J., Das Gupta, S.K. and Herzfeld, J. (9187) in Biophysical Studies of Retinal Proteins (Ebrey, T.G., Frauenfelder, H., Honig, B. and Nakanishi, K., eds.), pp. 133–134, University of Illinois Press, Urbana.
101 Ebrey, T.G., Frauenfelder, H., Honig, B. and Nakanishi, K. (eds.) (1987) Biophysical Studies of Retinal Proteins, University of Illinois Pres. Urbana.

102 Einterz, C.M., Hug, J.S., Lewis, J.W. and Kliger, D.S. (1990) Biochemistry, in press.
103 Einterz, C.M., Lewis, J.W. and Kliger, D.S. (1987) in Biophysical Studies of Retinal Proteins (Ebrey, T.G., Frauenfelder, H., Honig, B. and Nakanishi, K., eds.), pp. 282–286, University of Illinois Press, Urbana.
104 Eisenbach, M., Bakker, E.P., Korenstein, R. and Caplan, S.R. (1976) FEBS Lett. 71, 228–232.
105 Eisenstein, L., Lin, S.L., Dollinger, G., Termini, J., Odashima, K. and Nakanishi, K. (1987) in Biophysical Studies of Retinal Proteins (Ebrey, T.G., Freuenfelder, H., Honig, B. and Nakanishi, K., eds.), pp. 149–155, University of Illinois Press, Urbana.
106 El-Sayed, M.A. (1987) in Biophysical Studies of Retinal Proteins (Ebrey, T.G., Frauenfelder, H., Honig, B. and Nakanishi, K., eds.), pp. 174–180, University of Illinois Press, Urbana.
107 Engelhard, M., Gerwert, K., Hess, B., Kreitz, W. and Siebert, F. (1985) Biochemistry 24, 400–407.
108 Engelman, D.M. (1982) Biophys. J. 37, 187–188.
109 Engelman, D.M., Henderson, R., McLachlan, A.D. and Wallace, B.A. (1980) Proc. Natl. Acad. Sci. USA 77, 2023–2027.
110 Eyring, G. and Mathies, R. (1979) Proc. Natl. Acad. Sci. USA 76, 33–37.
111 Fang, J.M., Carriker, J.D., Balogh-Nair, V. and Nakanishi, K. (1983) J. Am. Chem. Soc. 105, 5162–5164.
112 Fodor, S.P.A., Ames, J.A., Gebhard, R., Van den Berg, E.M.M., Stoeckenius, W., Lugtenburg, J. and Mathies, R.A. (1988) Biochemistry 27, 7097–7101.
113 Fodor, S.P.A., Pollard, W.T., Gebhard, R., Van den Berg, E.M.M., Lugtenburg, J. and Mathies, R.A. (1988) Proc. Natl. Acad. Sci. USA 85, 2156–2160.
114 Foster, K.W. and Saranak, J. (1988) J. Am. Chem. Soc. 110, 6588–6589.
115 Foster, K.W., Saranak, J., Derguini, F., Zarrilli, G.R., Johnson, R., Okabe, M. and Nakanishi, K. (1989) Biochemistry 28, 819–824.
116 Foster, K.W., Saranak, J., Patel, N., Zarilli, G., Okabe, M., Kline, T. and Nakanishi, K. (1984) Nature 311, 756–759.
117 Foster, K.W., Saranak, J. and Zarrilli, G. (1988) Proc. Natl. Acad. Sci. USA 85, 6379–6383.
118 Freedman, K. and Becker, R.S. (1986) J. Am. Chem. Soc. 108, 1245–1251.
119 Freedman, K., Becker, R.S., Hannak, D. and Bayer, E. (1986) Photochem. Photobiol. 43, 291–295.
120 Fukumoto, J., Hopewell, W.D., Karvaly, B. and El-Sayed, M.A. (1981) Proc. Natl. Acad. Sci. USA 78, 252–255.
121 Genter, U.M., Gartner, W. and Siebert, F. (1988) Biochemistry 27, 7480–7488.
122 Gerwert, K. and Hess, B. (1987) in Biophysical Studies of Retinal Proteins (Ebrey, T.G., Frauenfelder, H., Honig, B. and Nakanishi, K., eds.), pp. 144–148, University of Illinois Press, Urbana.
123 Gillbro, T. and Sundstrom, V. (1983) Photochem. Photobiol. 37, 445–455.
124 Goldschmidt, C.R., Kalisky, O., Rosenfeld, T. and Ottolenghi, M. (1977) Biophys. J. 17, 179–183.
125 Goldschmidt, C.R., Ottolenghi, M. and Korenstein, R. (1976) Biophys. J. 16, 839–843.
126 Govindjee, R., Dancshazy, Z. and Ebrey, T.G. (1989) in Biomolecular Spectroscopy (Birge, R.R. and Mantsch, H.H., eds.), pp. 126–137, SPIE, Int. Soc. Opt. Eng., Bellingham, Washington.
127 Govindjee, R., Dancshazy, Z., Ebrey, T.G., Longstaff, C. and Rando, R.R. (1988) Photochem. Photobiol. 48, 493–496.
128 Govindjee, R., Ebrey, T.G. and Crofts, A.R. (1980) Biophys. J. 30, 231–242.
129 Green, B., Monger, T., Alfano, R., Anton, B. and Callender, R.H. (1977) Nature (London) 269, 179–180.
130 Grellmann, K.H., Livingston, R. and Pratt, D. (1962) Nature 193, 1258–1260.
131 Grieger, I. and Atkinson, G.H. (1985) Biochemistry 24, 5660–5665.
132 Groma, G.I., Szabo, G. and Varo, G. (1984) Nature 308, 557–558 (Letter).
133 Hackett, N.R., Stern, L.J., Chao, B.H., Kronis, K.A. and Khorana, H.G. (1987) J. Biol. Chem. 269, 9277–9284.
134 Hanamoto, J.H., Dupuis, P. and El-Sayed, M.A. (1984) Proc. Natl. Acad. Sci. USA 81, 7083–7087.
135 Harbison, G.S., Roberts, J.E., Herzfeld, J. and Griffin, R.G. (1988) J. Am. Chem. Soc. 110, 7221–7223.
136 Harbison, G.S., Smith, S.O., Pardoen, J.A., Courint, J.M.L., Lugtenburg, J., Herzfeld, J., Mathies, R.A. and Griffin, R.G. (1985) Biochemistry 24, 6955–6962.
137 Harbison, G.S., Smith, S.O., Pardoen, J.A., Winkel, J., Lugtenburg, J., Herzfeld, J., Mathies, R.A. and Griffin, R.G. (1984) Proc. Natl. Acad. Sci. USA 81, 1706–1709.
138 Hargrave, P.A. (1982) Prog. Retinal Res. 1, 1–51.
139 Hargrave, P.A., Mcdowell, J.H., Curtis, D.R., Wang, J.K., Juszczak, E., Fong, S.L., Rao, J.K.M. and Argos, R. (1983) Biophys. Struct. Mech. 9, 235–244.
140 Hargrave, P.A., McDowell, J.H., Feldman, R.J., Atkinson, P.H., Mohana, Rao, J.K. and Argos, P. (1984) Vision Rev. 24, 1487–1499.
141 Hayward, B.S., Grano, D.A., Glaeser, R.M. and Fisher, K.A. (1978) Proc. Natl. Acad. Sci. U.S.A. 75, 4320–4324.
142 Henderson, R. (1975) J. Mol. Biol. 93, 123–138.
143 Henderson, R. (1977) Annu. Rev. Biophys. Bioeng. 6, 87–109.
144 Henderson, R. and Univin, P.N.T. (1975) Nature 237, 28–32.
145 Heyn, M.P., Braun, D., Dencher, N.A., Fahr, A., Holz, M., Lindau, M., Seiff, F., Wallat, I. and Westerhausen, J. (1988) Ber. Bunsenges. Phys. Chem. 92, 1045–1050.
146 Heyn, M.P., Westerhausen, J., Wallat, I. and Seiff, F. (1988) Proc. Natl. Acad. Sci. USA 85, 2146–2150.
147 Hildebrandt, P. and Stockburger, M. (1984) Biochemistry 23, 5539–5548.
148 Hirsch, M.D., Marcus, M.A., Lewis, A., Mahr, H. and Frigo, N. (1976) Biophys. J. 16, 1399–1409.
149 Hoffmann, W., Graca-Miguel, M., Barnard, P. and Chapman, D. (1979) FEBS Lett. 95, 31–34.
150 Hong, F.T. and Okajima, R.L. (1987) in Biophysical Studies of Retinal Proteins (Ebrey, T.G., Frauenfelder, H., Honig, B. and Nakanishi, K., eds.), pp. 188–198, University of Illinois Press, Urbana.
151 Honig, B. (1981) Ann. NY Acad. Sci. 376, 269–280.
152 Honig, B. (1982) in Biological Events Probed by Ultrafast Laser Spectroscopy (Alfano, R.R., ed.), pp. 281–296. Academic Press, New York.
153 Honig, B. (1987) in Biophysical Studies of Retinal Proteins (Ebrey, T.G., Frauenfelder, H., Honig, B. and Nakanishi, K., eds.), pp. 212–218, University of Illinois Press, Urbana.
154 Honig, B., Dinur, U., Birge, R.R. and Ebrey, T.G. (1980) J. Am. Chem. Soc. 102, 488–494.
155 Honig, B., Dinur, U., Nakanishi, K., Balogh-Nair, V., Gawinowicz, M.A., Arnaboldi, M. and Motto, M.G. (1979) J. Am. Chem. Soc. 101, 7084–7086.
156 Honig, B., Ebrey, T., Callender, R.H., Dinur, U. and Ottolenghi, M. (1979) Proc. Natl. Acad. Sci. USA 76, 2503–2507.
157 Honig, B., Greenberg, A.D., Dinur, V. and Ebrey, T.G. (1976) Biochemistry 15, 4593–4599.
158 Honig, B., Hudson, B., Sykes, B.D. and Karplus, M. (1971) Proc. Natl. Acad. Sci. USA 68, 1289–1293.
159 Honig, B., Warshel, A. and Karplus, M. (1975)Acc. Chem. Res. 8, 92–100.
160 Hsieh, C.L., Nagumo, M., Nicol, M. and El-Sayed, M.A. (1981) J. Phys. Chem. 85, 2714–2717.
161 Hubbard, R. (1958) J. Gen. Physiol. 42, 259–280.
162 Hubbard, R. (1966) J. Biol. Chem. 241, 1814–1818.

163 Hudson, B. and Kohler, B.E. (1974) Annu. Rev. Phys. Chem. 25, 437–460.
164 Hudson, B.S. and Kohler, B.E. (1973) J. Chem. Phys. 59, 4984–5002.
165 Hug, S.J., Lewis, J.W., Einterz, C.M., Thorgeirsson, T.E. and Kliger, D.S. (1990) Biochemistry, in press.
166 Hug, S.J., Lewis, J.W. and Kliger, D.S. (1988) J. Am. Chem. Soc. 110, 1998–1999.
167 Huppert, D., Rentzepis, P.M. and Kliger, D.S. (1977) Photochem. Photobiol. 25, 193–197.
168 Hurley, J.B. and Ebrey, T.G. (1978) Biophys. J. 22, 49–66.
169 Hurley, J.B., Ebrey, T.G., Honig, B. and Ottolenghi, M. (1977) Nature (Lond.) 270, 540–542.
170 Ippen, E.P., Shank, C.V., Lewis, A. and Marcus, M.A. (1978) Science (Washington, DC) 200, 1279–1281.
171 Iwasa, T., Tokunaga, F., Yoshizawa, T. and Ebrey, T.G. (1980) Photochem. Photobiol. 31, 83–86.
172 Iwasa, T., Tokunaga, F. and Yoshizawa, T.I. (1980) Biophys. Struct. Mech. 6, 253–270.
173 Jap, B.K., Maestre, M.F., Harward, S.B. and Glaeser, R.M. (1983) Biophys. J. 43, 81–89.
174 Kakitani, H., Kakintani, T., Rodman, H. and Honig, B. (1983) J. Phys. Chem. 87, 3620–3628.
175 Kakitani, H., Kakitani, T., Rodman, H. and Honig, B. (1985) Photochem. Photobiol. 41, 471–479.
176 Kalisky, O. and Ottolenghi, M. (1982) Photochem. Photobiol. 35, 109–115.
177 Keszthelyi, L. and Ormos, P. (1980) FEBS Lett. 109, 189–193.
178 Khorana, H.G., Gerber, G.E., Herlihy, W.C., Gray, C.P., Anderegg, R.J., Nihei, K. and Biemann, K. (1979) Proc. Natl. Acad. Sci. USA 76, 5046–5050.
179 Kobayashi, T. (1979) FEBS Lett. 106, 313–316.
180 Kolling, E., Gartner, W., Oesterhelt, D. and Ernst, L. (1984) Angew. Chem. Int. Ed. Engl. 23, 81–82.
181 Korenstein, R., Hess, B. and Kuschmitz, D. (1978) FEBS Lett. 93, 266–270.
182 Kouyama, T., Kouyama, A.N., Ikegami, A., Mathew, M.K. and Stoeckenius, W. (1988) Biochemistry 27, 5855–5863.
183 Kryukov, P.G., Lazrev, Y.A., Matveetz, Y.A., Terpugov, E.L., Chekulaeva, L.N. and Sharkov, A.V. (1981) Stud. Biophys. 83, 101–108.
184 Kuschmitz, D. and Hess, B. (1982) FEBS Lett. 138, 137–140.
185 Lanyi, J.K. (1978) Microbiol. Rev. 42, 682–712.
186 Lanyi, J.K. (1981) Trends Biochem. Sci. 6, 60–62.
187 Lanyi, J.K. (1984) in New Comprehensive Biochemistry (Ernster, L., ed.), pp. 315–350, North-Holland, Amsterdam.
188 Lanyi, J.K. (1986) Annu. Rev. Biophys. Chem. 15, 11–28.
189 Law, W.C., Kim, S. and Rando, R.R. (1989) J. Am. Chem. Soc. 111, 793–795.
190 Lee, D.C., Harward, J.A., Restall, C.J. and Chapman, D. (1985) Biochemistry 24, 4364–4373.
191 Lewis, J.W., Einterz, C.M., Hug, S.J. and Kliger, D.S. (1989) Biophys. J., in press.
192 Li, Q.Q., Govindjee, R. and Ebrey, T.G. (1984) Proc. Natl. Acad. Sci. 81, 7091–7082.
193 Liebman, P.A., Parker, K.R. and Dratz, E.A. (1987) Annu. Rev. Physiol. 49, 965–991.
194 Lin, S.W., and Mathies, R.A. (1989) Biophys. J. 56, 653–660.
195 Litvin, F.F., Balashov, S.P. and Sineschekow, V.A. (1975) Bioorganicheskaya Khimiya (USSR) 1, 1767–1777.
196 Liu, R.S.H. and Asato, A.E. (1982) Methods Enzymol. 88, 506–516.
197 Liu, R.S.H. and Asato, A.E. (1984) Tetrahedron 40, 1931–1969.
198 Liu, R.S.H. and Asato, A.E. (1985) Proc. Natl. Acad. Sci., USA 82, 259–263.
199 Liu, R.S.H., Denny, M., Grodowski, M. and Asato, A.E. (1979) Nouv. J. Chem. 3, 503–505.
200 Liu, R.S.H., Denny, M., Zingoni, J.P., Mead, D., Matsumoto, H. and Asato, A.E. (1987) in Biophysical Studies of Retinal Proteins (Ebrey, T.G., Frauenfelder, H., Honig, B. and Nakanishi, K., eds.), pp. 59–63, University of Illinois Press, Urbana.
201 Liu, R.S.H., Matsumoto, H., Asato, A.E., Denny, M., Shichida, Y., Yoshizawa, T. and Dahlquist, F.W. (1981) J. Am. Chem. Soc. 103, 7195–7201.
202 Liu, R.S.H., Mead, D. and Asato, A.E. (1985) J. Am. Chem. Soc. 107, 6609–6614.
203 Longstaff, C., Calhoon, R.D. and Rando, R.R. (1986) Proc. Natl. Acad. Sci. USA 83, 4209–4213.
204 Longstaff, C. and Rando, R.R. (1987) Biochemistry 26, 6107–6113.
205 Longstaff, C., Seckler, B., Calhoon, R.D. and Rando, R.R. (1987) in Biophysical Studies of Retinal Proteins (Ebrey, T.G., Frauenfelder, H., Honig, B. and Nakanishi, K., eds.), pp. 64–70, University of Illinois Press, Urbana.
206 Lopez-Garriga, J.J., Babcock, G.T. and Harrison, J.F. (1986) J. Am. Chem. Soc. 108, 7241–7251.
207 Lopez-Garriga, J.J., Babcock, G.T. and Harrison, J.F. (1986) J. Am. Chem. Soc. 108, 7131–7133.
208 Loppnow, G.R., Barry, B.A. and Mathies, R.A. (1989) Proc. Natl. Acad. Sci. USA 86, 1515–1518.
209 Lozier, R.H., Bogomolni, R.A. and Stoeckenius, W. (1975) Biophys. J. 15, 955–962.
210 Lugtenburg, J., Muradin-Szweykowska, M., Heeremans, C. and Pardoen, J.A. (1986) J. Am. Chem. Soc. 108, 3104–3105.
211 Lukton, D. and Rando, R.R. (1984) J. Am. Chem. Soc. 106, 258–259.
212 Mao, B., Ebrey, T.G. and Crouch, R. (1980) Biophys. J. 29, 247–256.
213 Mao, B., Tsuda, M., Ebrey, T., Akita, H., Balogh-Nair, V. and Nakanishi, K. (1981) Biophys. J. 35, 543–546.
214 Marcus, M.A. and Lewis, A. (1977) Science (Washington, DC) 195, 1328–1330.
215 Marinetti, T. (1987) Biophys. J. 51, 875–881.
216 Marinetti, T. (1987) Biophys. J. 52, 115–121.
217 Marinetti, T. and Mauzerall, D. (1983) Proc. Natl. Acad. Sci. USA 80, 178–180.
218 Mateescu, G.D., Copan, W.G., Muccio, D.D., Waterhouse, D.V. and Abrahamson, E.W. (1983) in Proceedings of the International Symposium on Synthesis and Applications of Isotopically Labeled Compounds (Duncan, W.P. and Susan, A.P., eds.), pp. 123–132, Elsevier, Amsterdam.
219 Mathies, R. (1982) Methods Enzymol. 88, 633–643.
220 Mathies, R.A., Brito Cruz, C.H., Polalrd, W.T. and Shank, C.V. (1988) Science 240, 777.
221 Mathies, R.A., Smith, S.O. and Lugtenburg, J. (1987) in Biophysical Studies of Retinal Proteins (Ebrey, T.G., Frauenfelder, H., Honig, B. and Nakanishi, K., eds.), pp. 126–132, University of Illinois Press, Urbana.
222 Matuoka, M., Shichida, Y. and Yoshizawa, T. (1984) Biochim. Biophys. Acta 765, 38–42.
223 McMaster, E. and Lewis, A. (1988) Biochem. Biophys. Res. Commun. 156, 86.
224 Metzler, D.E. and Harris, C.M. (1978) Vision Res. 18, 1417–1420.
225 Michel, H. and Oesterhelt, D. (1980) Biochemistry 19, 4615–4619.
226 Michel, H. and Oesterhelt, D. (1980) Biochemistry 19, 4607–4614.
227 Mogi, T., Stern, L.J., Hackett, N.R. and Khorana, H.G. (1987) Proc. Natl. Acad. Sci. USA 84, 5595–5599.
228 Mogi, T., Stern, L.J., Marti, T., Chao, B.H. and Khorana, H.G. (1988) Proc. Natl. Acad. Sci. USA 85, 4148–4152.
229 Monger, T., Alfano, R.R. and Callender, R.H. (1979) Biophys. J. 27, 105–115.
230 Murray, L.P. and Birge, R.R. (1985) Canad. J. Chem. 63, 1967–1971.
231 Murray, L.P., Findsen, L.A., Pierce, B.M. and Birge, R.R. (1986)

in Fluorescence in the Biomedical Sciences (Taylor, D.L., Waggoner, A., Lannie, R., Murphy, R. and Birge, R.R., eds.), pp. 105–127, Alan R. Liss, New York.
232 Nabedryk, E., Bardin, A.M. and Breton, J. (1985) Biophys. J. 48, 873–876.
233 Nakanishi, K. (1987) in Biophysical Studies of Retinal Proteins (Ebrey, T.G., Frauenfelder, H., Honig, B. and Nakanishi, K., eds.), pp. 1–15, University of Illinois Press, Urbana.
234 Nakanishi, K., Balogh-Nair, V., Arnaboldi, M., Tsujimoto, K. and Honig, R. (1980) J. Am. Chem. Soc. 102, 7945–7947.
235 Nathans, J. and Hogness, D.S. (1983) Cell 34, 807–814.
236 Nathans, J. and Hogness, D.S. (1984) Proc. Natl. Acad. Sci. USA 81, 4851–4855.
237 Nathans, J., Thomas, D. and Hogness, D.S. (1986) Science 232, 193–202.
238 Nuss, M.C., Zinth, W., Kaiser, W., Kolling, E. and Oesterhelt, D. (1985) Chem. Phys. Lett. 117, 1–7.
239 Oesterhelt, D., Hegemann, P. and Tittor, J. (1985) EMBO J. 4, 2351–2356.
240 Oesterhelt, D. and Hess, B. (1973) Eur. J. Biochem. 37, 316–326.
241 Oesterhelt, D. and Schuhmann, L. (1974) FEBS Lett. 44, 262–265.
242 Oesterhelt, D. and Stoeckenius, W. (1971) Nature, New Biol. 233, 149–152.
243 Oesterhelt, D. and Stoeckenius, W. (1974) Methods Enzymol. 31, 667–678.
244 Ohno, K., Govindjee, R. and Ebrey, T.G. (1983) Biophys. J. 43, 251–254.
245 Ormos, P., Reinisch, L. and Keszthelyi, L. (1983) Biochim. Biophys. Acta 722, 471–479.
246 Oseroff, A.R. and Callender, R.H. (1974) Biochemistry 13, 2443–4348.
247 Ovchinnikov, Y.A. (1982) FEBS Lett. 148, 179–191.
248 Ovchinnikov, Y.A., Abdulaev, N.G., Feigina, M.Y., Kiselev, A.V. and Lobanov, N.A. (1979) FEBS Lett. 100, 219–224.
249 Palings, J., Pardoen, J.A., Van der Berg, E., Winkel, C., Lungtenburg, J. and Mathies, R.S. (1987) Biochemistry 26, 2544–2556.
250 Pande, A.J., Callender, R.H., Ebrey, T.G. and Tsuda, M. (1984) Biophys. J. 45, 573–576.
251 Peters, K.S., Applebury, M.L. and Rentzepis, P.M. (1977) Proc. Natl. Acad. Sci. (USA) 74, 3119–3123.
252 Polland, H.J., Franz, M.A., Zinth, W., Kaiser, W., Kolling, E. and Oesterhelt, D. (1984) Biochim. Biophys. Acta 767, 635–639.
253 Polland, H.J., Franz, M.A., Zinth, W., Kaiser, W., Kolling, E. and Oesterhelt, D. (1986) Biophys. J. 49, 651–662.
254 Polland, H.J. and Zinth, W. (1984) Optics Commun. 50, 194–400.
255 Pollard, W.T., Cruz, C.H.B., Shank, C.V. and Mathies, R.A. (1989) J. Chem. Phys. 90, 199–208.
256 Ponder, M. (1983) Ph.D., University of California, Berkeley.
257 Rafferty, C.N. and Shichi, H. (1981) Photochem. Photobiol. 33, 229–234.
258 Rando, R.R. and Chang, A. (1983) J. Am. Chem. Soc. 105, 2879–2882.
259 Renk, G., Goletz, P., Crouch, R.K., Chung-Ho, C., Govindjee and Ebrey, T.G. (1987) in Biophysical Studies of Retinal Proteins (Ebrey, T.G., Freuenfelder, H., Honig, B. and Nakanishi, K., eds.), pp. 80–85, University of Illinois Press, Urbana.
260 Roepe, P., Ahl, P.L., DasGupta, S.K., Herzfeld, J. and Rothschild, K.J. (1987) Biochemistry 26, 6696–6707.
261 Roepe, P., Ahl, P.L., Herzfeld, J., Lugtenburg, J. and Rothschild, K.J. (1988) J. Biol. Chem. 263, 5110–5117.
262 Roepe, P., Gray, D., Lugtenburg, J., van den Berg, E.M.M., Herzfeld, J. and Rothschild, K.J. (1988) J. Am. Chem. Soc. 110, 7223–7224.
263 Rosenfeld, T., Honig, B. and Ottolenghi, M. (1977) Pure Appl. Chem. 49, 341–351.
264 Rosenfeld, T., Honig, B., Ottolenghi, M., Hurley, J.B. and Ebrey, T.G. (1977) Pure Appl. Chem. 49, 341–351.
265 Rothschild, K.J., Argade, P.V., Earnest, T.N., Huang, K.S., London, E., Liao, M.-J., Bayley, H., Khorana, H.G. and Herzfeld, J. (1982) J. Biol. Chem. 257, 8592–8595.
266 Rothschild, K.J., Braiman, M.S., Bousche, O. and He, Y.W. (1989) in Biomolecular Spectroscopy (Birge, R.R. and Mantsch, H.H., eds.), pp. 44–48, The International Society for Optical Engineering, Bellingham, Washington.
267 Rothschild, K.J, Cantore, W.A. and Marrero, H. (1983) Science 219, 1333–1335.
268 Rothschild, K.J., Marrero, H., Braiman, M. and Mathies, R. (1984) Photochem. Photobiol. 40, 675–679.
269 Rothschild, K.J., Roepe, P., Ahl, P.L., Earnest, T.N., Bogomolni, R.A., Das Gupta, S.K., Mulliken, C.M. and Herzfeld, J. (1986) Proc. Natl. Acad. Sci. USA 83, 347–351.
270 Rothschild, K.J., Roepe, P. and Gillespie, J. (1985) Biochim. Biophys. Acta 808, 140–148.
271 Rothschild, K.J., Roepe, P., Lugtenburg, J. and Pardoen, J.A. (1984) Biochemistry 23, 6103–6109.
272 Rowan, R., Warshel, A., Sykes, B.D. and Karplus, M. (1974) Biochemistry 13, 970–981.
273 Saibil, S.H., Chabre, M. and Worcester, D. (1976) Nature 262, 266–270.
274 Sakmar, T.P., Franke, R.R. and Khorana, H.G. (1989) Proc. Natl. Acad. Sci. USA 86, 8309–8313.
275 Sandorfy, C., Lussier, L.S., Thanh, H.L. and Vocelle, D. (1987) in Biophysical Studies of Retinal Proteins (Ebrey, T.G., Frauenfelder, H., Honig, B. and Nakanishi, K., eds.), pp. 247–251, University of Illinois Press, Urbana.
276 Sandorfy, C. and Vocelle, D. (1986) Can. J. Chem. 64, 2251–2266.
277 Schick, G.A., Cooper, T.M., Holloway, R.A., Murray, L.P. and Birge, R.R. (1987) Biochemistry 26, 2556–2562.
278 Schreckenbach, T., Walckhoff, B. and Oesterhelt, D. (1978) Photochem. Photobiol. 28, 205–211.
279 Schreckenbach, T., Walckhoff, B. and Oesterhelt, D. (1978) J. Am. Chem. Soc. 17, 5353–5359.
280 Schulten, K., Schulten, Z. and Tavan, P. (1984) in Information and Energy Transduction in Biological Membranes (Bolis, L., Helmrich, E.J.M. and Passow, H., eds.), pp. 113–131, Alan R. Liss, New York.
281 Schulten, K. and Tavan, P. (1978) Nature (London) 272, 85–86.
282 Seiff, F., Wallat, I., Ermann, P. and Heyn, M.P. (1985) Proc. Natl. Acad. Sci. USA 82, 3227–3231.
283 Sharkov, A.V., Matveetz, Y.A., Chekalin, S.V., Konyashchenko, A.V., Krekhov, O.M. and Rootskoy, B.Y. (1983) Photochem. Photobiol. 38, 108–111.
284 Sharkov, A.V., Pakulev, A.V., Chekalin, S.V. and Matveetz, Y.A. (1985) Biochim. Biophys. Acta 808, 94–102.
285 Sheves, M., Albeck, A., Friedman, N. and Ottolenghi, M. (1986) Proc. Natl. Acad. Sci. USA 83, 3262–3266.
286 Sheves, M., Albeck, A., Ottolenghi, M., Bovee-Geurts, P.H.M., De Grip, W.J., Einterz, C.M., Lewis, J.W., Schaechter, L.E. and Kliger, D.S. (1986) J. Am. Chem. Soc. 108, 6440–6441.
287 Sheves, M., Friedman, N., Albeck, A. and Ottolenghi, M. (1985) Biochemistry 24, 1260–1265.
288 Sheves, M., Nakanishi, K. and Honig, B. (1979) J. Am. Chem. Soc. 101, 7086–7088.
289 Shichi, H. (ed.) (1983) Biochemistry of Vision, Academic Press, New York.
290 Shichida, Y. (1986) Photobiochem. Photobiophys. 13, 287–307.
291 Shichida, Y., Nakamura, K., Yoshizawa, T., Trehan, A., Denny, M. and Liu, R.S.H. (1988) Biochemistry 27, 6495–6499.
292 Shichida, Y., Yoshizawa, T., Kobayashi, T., Ohtani, H. and Nagakura, S. (1977) FEBS Lett. 80, 214–216.
293 Siebert, F. and Mantele, W. (1983) Eur. J. Biochem. 130, 565–573.
294 Siebert, F., Mantele, W. and Gerwert, K. (1983) Eur. J. Biochem. 136, 119–127.
295 Smith, S.O. (1985) Ph.D., University of California, Berkeley.

296 Smith, S.O., Braiman, M.S., Myers, A.B., Pardoen, J.A., Courtin, J.M.L., et al. (1987) J. Am. Chem. Soc. 109, 3108–3125.
297 Smith, S.O., Copie, V., Raleigh, D.P., Griffin, R.G., Palings, I., Mathies, R.A., Courtin, J., Winkel, C. and Lugtenburg, J. (1987) in Biophysical Studies of Retinal Proteins (Ebrey, T.G., Freuenfelder, H., Honig, B. and Nakanishi, K., eds.), pp. 226–232, University of Illinois Press, Urbana.
298 Smith, S.O., Harbison, G.S., Raleigh, D.P., Griffin, R.G., Winkel, C., Pardoen, J.A., Lugtenburg, J. and Herzfeld, J. (1987) in Biophysical Studies of Retinal Proteins (Ebrey, T.G., Frauenfelder, H., Honig, B. and Nakanishi, K., eds.), pp. 219–225, University of Illinois Press, Urbana.
299 Smith, S.O., Hornung, I., Van der Steen, R., Pardoen, J.A., Braiman, M.S., Lugtenburg, J. and Mathies, R.A. (1986) Proc. Natl. Acad. Sci. USA 83, 967–971.
300 Smith, S.O., Lugtenburg, J. and Mathies, R.A. (1985) J. Membr. Biol. 85, 95–109.
301 Smith, S.O., Myers, A.B., Mathies, R.A., Pardoen, J.A., Winkel, C., Van Den Berg, E.M.M. and Lugtenburg, J. (1985) Biophys. J. 47, 653–664.
302 Smith, S.O., Myers, A.B., Pardoen, J.A., Winkel, C., Mulder, P.P.J., Lugtenburg, J. and Mathies, R. (1984) Proc. Natl. Acad. Sci. USA 81, 2055–2059.
303 Smith, S.O., Palings, J., Copie, V., Raleigh, D.R., Courtin, J., Pardoen, J.A., Lugtenburg, J., Mathies, R.A. and Griffin, R.G. (1987) Biochemistry 26, 1606–1611.
304 Smith, S.O., Pardoen, J.A., Lugtenburg, J. and Mathies, R.A. (1987) J. Phys. Chem. 91, 804–819.
305 Spudich, J.L. and Bogomolni, R.A. (1987) in Biophysical Studies of Retinal Proteins (Ebrey, T.G., Frauenfelder, H., Honig, B. and Nakanishi, K., eds.), pp. 24–30, University of Illinois Press, Urbana.
306 Spudich, J.L., McCain, D.A., Nakanishi, K., Okabe, M., Shimizu, N., Rodman, H., Honig, B. and Bogomolni, R.A. (1986) Biophys. J. 49, 479–483.
307 Stern, D. and Mathies, R. (1985) in Proceedings of the Proceedings of the 2nd International Conference Emil-Warburg Symposium (Laubereau, A. and Stockburger, M., eds.), pp. 250–254, Springer-Verlag, Berlin.
308 Stieve, H. (1984) The Molecular Mechanism of Photoreception, Springer-Verlag, New York.
309 Stockburger, M., Klusmann, W., Gattermann, H., Massig, G. and Peters, R. (1979) Biochemistry 18, 4886–4900.
310 Stoeckenius, W. and Bogomolni, R. (1982) Annu. Rev. Biochem. 52, 587–616.
311 Stoeckenius, W., Lozier, R.H. and Bogomolni, R. (1979) Biochim. Biophys. Acta 505, 215–278.
312 Stryer, L. (1986) Annu. Rev. Neurosci. 9, 87–119.
313 Suzuki, T. and Callender, R.H. (1981) Biophys. J. 34, 261–265.
314 Tavan, P. (1988) Phys. Chem. 92, 1040–1045.
315 Tavan, P. and Schulten, K. (1986) Biophys. J. 50, 81–89.
316 Tavan, P., Schulten, K. and Oesterhelt, D. (1985) Biophys. J. 47, 415–430.
317 Terner, J., Hsieh, C.L., Burns, A.R. and El-Sayed, M.A. (1979) Proc. Natl. Acad. Sci. USA 76, 3046–3050.
318 Trissl, H.W., Gartner, W. and Leible, W. (1989) Chem. Phys. Lett. 158, 515–518.
319 Tsuda, M., Glaccum, M., Nelson, B. and Ebrey, T.G. (1980) Nature (Lond.) 287, 351–353.
320 Van der Steen, R., Biesheuvel, P.L., Mathies, R.A. and Lugtenburg, J. (1986) J. Am. Chem. Soc. 108, 6410–6411.
321 Waddell, W.H., Crouch, R., Nakanishi, K. and Turro, N.J. (1976) J. Am. Chem. Soc. 98, 4189–4192.
322 Waddell, W.H., Schaffer, A.M. and Becker, R.S. (1977) J. Am. Chem. Soc. 99, 8456–8460.
323 Warshel, A. (1976) Nature 260, 679–683.
324 Warshel, A. and Barboy, N. (1982) J. Am. Chem. Soc. 104, 1469–1676.
325 Weiss, R.M. and Warshel, A. (1979) J. Am. Chem. Soc. 101, 6131–6133.
326 Witkovsky, P., Engbretson, G.A. and Ripps, H. (1978) J. Gen. Physiol. 72, 821–836.
327 Xie, A.H., Nagle, J.F. and Lozier, R.H. (1987) Biophys. J. 51, 627–635.
328 Yoshizawa, T., Matsumoto, H., Horiuchi, K., Shichida, Y., Ito, M., Kodama, A. and Tsukida, K. (1987) in Biophysical Studies of Retinal Proteins (Ebrey, T.G., Frauenfelder, H., Honig, B. and Nakanishi, K., eds.), pp. 287–292, University of Illinois Press, Urbana.
329 Yoshizawa, T., Shichida, Y. and Matuoka, S. (1984) Vision Res. 24, 1455–1463.
330 Yoshizawa, T. and Wald, G. (1963) Nature 197, 1279–1286.
331 Zhang, C.F. and Birge, R.R. (1990) J. Chem. Phys., in press.